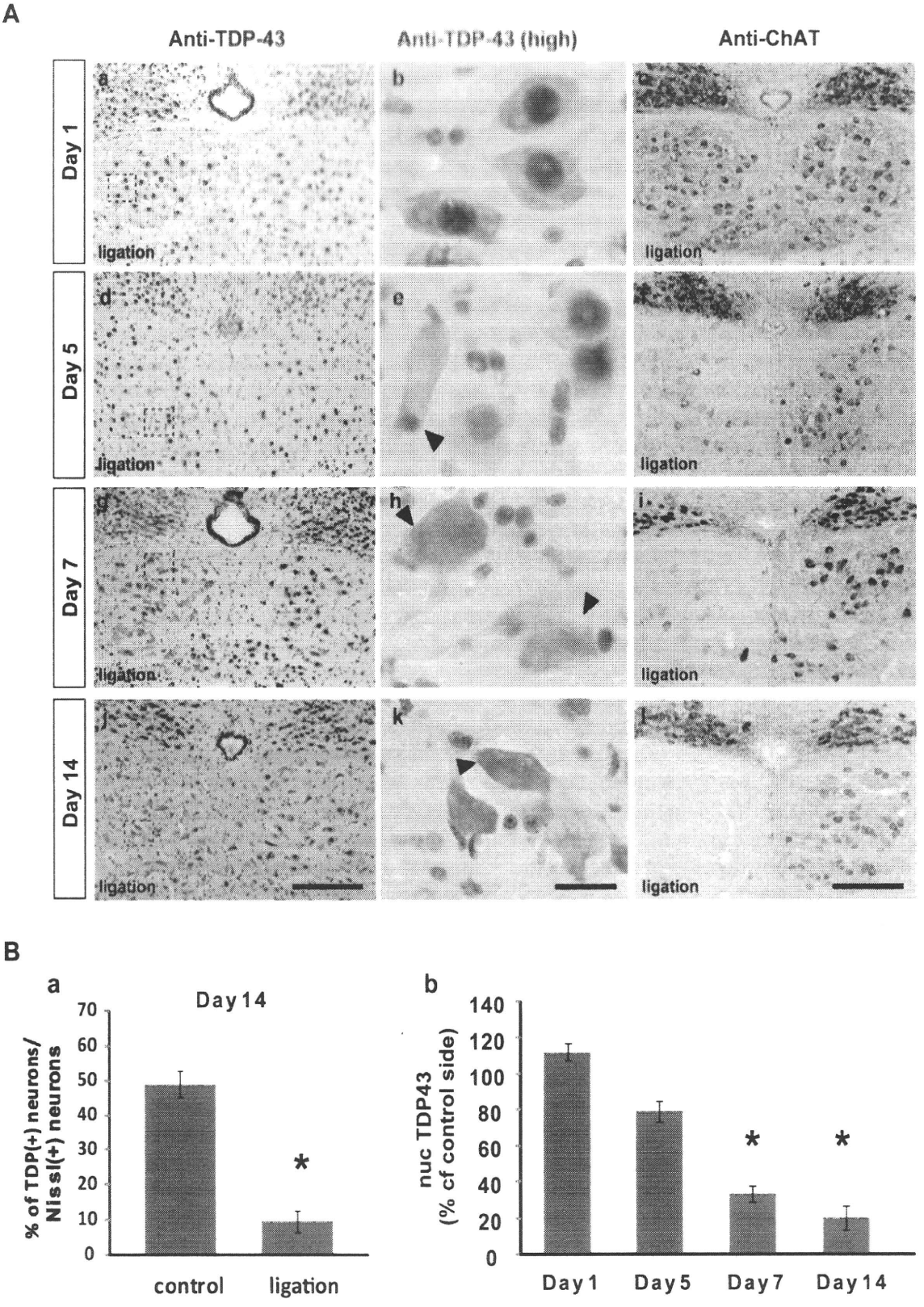

Fig. 1. Nerve ligation of hypoglossal nerves induced a gradual reduction in nuclear TDP-43 and in choline acetyltransferase (ChAT) expression (A) Immunohistochemistry of lower brainstem slices at the level of area postrema of adult C57Bl/6 mice 1, 5, 7 and 14 days after nerve ligation. Sections were stained with rabbit polyclonal anti-TDP-43 antibody (left columns, a, d, g, j, middle column, b, e, h, k, with higher magnification) and or goat polyclonal anti-ChAT (right columns, c, f, i, l). Nissl staining was conducted for counter-staining (blue). The magnified area was indicated by the dot line. The occasional cytosolic TDP-43 staining was indicated by arrowheads. Note that loss of TDP-43 staining was preceded by downregulation of ChAT, and was most prominent on day 7–14. Scale bar=200 μm for a, c, d, f, g, i, j, l; 20 μm for b, e, h, k. (B) Quantification of hypoglossal nucleus with normal TDP-43 staining 1, 5, 7 and 14 days after nerve ligation. Number of hypoglossal neurons harboring normal TDP-43 staining and that of Nissl-positive neurons were counted from four mice (three slices per mouse). (a) Number of hypoglossal neurons harboring normal TDP-43 staining and that of Nissl-positive neurons 14 days after ligation were counted from four mice (three slices per mouse), and percentage of TDP-positive per Nissl-positive neurons were obtained. Graph bars express mean±standard mean of error (SEM; $n=3$). * $P<0.01$ by student's t-test. (b) Time-line of the redistribution of TDP-43. The percentage of TDP-positive per Nissl-positive neurons of the ligation side to those of the control side were obtained. Graph bars express mean ± standard mean of error (SEM; $n=3$–4). * $P<0.01$ vs. Days, 1 and 5 by one way ANOVA of Bonferroni test.

RESULTS

Permanent ligation of the hypoglossal nerves eliminated nuclear TDP-43 in parallel to choline acetyltransferase (ChAT) expression

Mislocalization of TDP-43 is a pathological characteristic of sporadic and SOD1-unrelated familial ALS. However, it is unclear whether the mislocalization or nuclear reduction of TDP-43 is a primary or a secondary event to an unidentified cause. We investigated the effect of axonal damage, which has been implicated in ALS pathogenesis (Julien, 2001), on the redistribution of TDP-43. The hypoglossal nerve was chosen for this study because of its pure motor neuron properties and its exclusive vulnerability in ALS. Moreover, we simultaneously performed immunostaining for ChAT, since the relationship between axonal injury and ChAT expression has been intensively studied. Previous reports indicated that ChAT expression after axonal injury is transiently depressed at 7–14 days and returns to normal one month later (Lams et al., 1988; Matsuura et al., 1997), supposedly reflecting the regeneration or the functional recovery of adult cholinergic neurons (Maeda et al.,

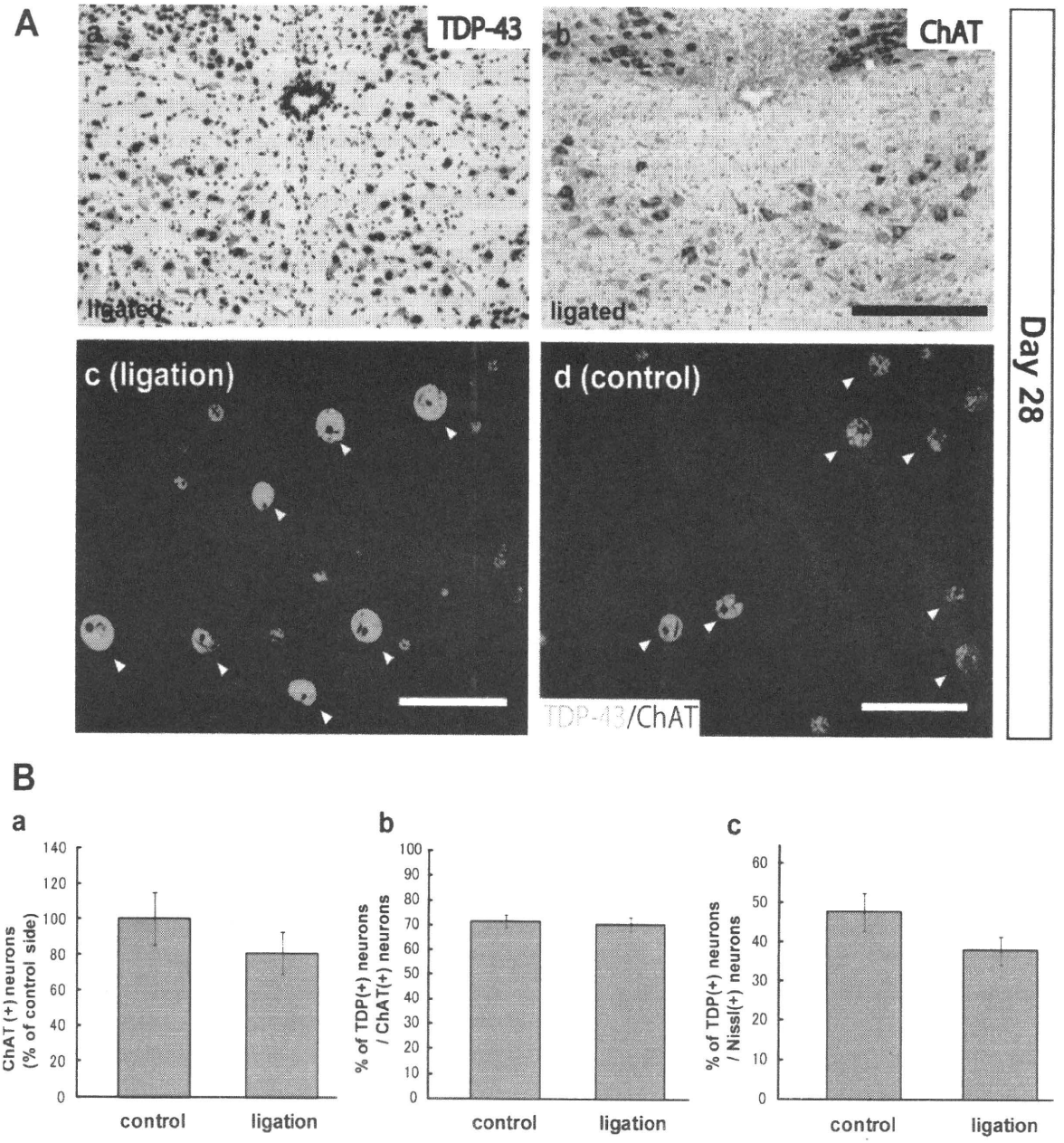

Fig. 2. Recovery of nuclear staining of TDP-43 on day 28 after nerve ligation (A) (a, b) Immunohistochemistry (DAB colorization) of brainstem slices 28 days after ligation using antibodies against TDP-43 (Proteintech, a) and ChAT (b) with Nissl counterstain. Scale bar=200 μm. (c, d) Confocal micrographs of double immunofluorescence of ligated (c) or untreated (d) side on day 28, using goat polyclonal anti-ChAT (red) and rabbit polyclonal TDP-43 (green) antibodies. Note that neurons with ChAT immunoreactivity contain normal nuclear TDP-43. Scale bar=50 μm. (B) The population of the hypoglossal nucleus on day 28 by the number of ChAT-positive neurons (a), TDP-43-positive/ChAT-positive neurons (b), and TDP-43-positive/Nissl-positive neurons (c). Neurons were counted under the microscope or in confocal micrographs from three slices per mouse (n=3). Data in a stands for mean±SEM (n=3) of the percentage of counted neurons in comparison with the control side. Each bar in each figure represents mean±SEM of percentage of ChAT-positive neurons (a), TDP-43-positive neurons per ChAT-positive (b) or per Nissl-positive neurons (c), (n=3).

2004). As shown in Fig. 1A-a gradual decrease in nuclear staining of TDP-43 was observed from day 5, and most prominently on days 7–14 (Fig. 1A, left and middle columns). In these neurons with reduced nuclear TDP-43, cytosolic staining was occasionally observed (arrowheads). However, no obvious aggregates were detected. In contrast to TDP-43, ChAT staining at the ligation side began to diminish on day 2 (not shown) and almost disappeared from day 7–14 (Fig. 1A, right column), consistent with a previous report (Matsuura et al., 1997).

The counting of nuclear TDP-43-positive per Nissl-positive neurons at day 14 after ligation revealed that there was a significant reduction in TDP-43-positive neurons by 9.7% on the ligation side and 49.0% on the unligated side after nerve ligation (Fig. 1B-a). It should be noted that unilateral ligation of the hypoglossal nerve affected nuclear staining of TDP-43 even on the contralateral side, especially near the midline, while almost 100% of the hypoglossal nucleus is clearly TDP-43-positive without ligation surgery (not shown). This correlated to a partial loss of ChAT staining at the contra-lateral side (Fig. 1A-i, I). Next, the percentage of the neurons with normal TDP-43 (nuc TDP43) to the control side was obtained. As shown in Fig. 1B, the number of nuclear TDP-43-/Nissl-positive neurons gradually diminished in a time-dependent manner. On days 7 and 14, there was a prominent reduction in TDP-43-positive neurons to 32.7% and 19.8% of the control side, respectively (Fig. 1B-b). We also confirmed that loss of nuclear TDP-43 is not related to impaired immunoreactivity related to the injury, since immunostaining with anti-TGN38 antibody showed similar reactivity between control and ligation sides (Fig. S1, A).

We further investigated TDP-43 staining at the chronic stage following axonal ligation together with the ChAT staining. In accordance with the previous reports, the number of ChAT-positive neurons returned to 80% of that on the control side 28 days after ligation (Figs. 2A-b, 2B-a). In addition, most ChAT positive neurons showed normal TDP-43 staining on day 28 (Fig. 2A-c). The quantification from double immunofluorescent confocal micrographs revealed that there is no difference in the percentage of TDP-43-positive neurons in ChAT-positive neurons between the ligated and the untreated side (Fig. 2B-b). Although the percentage of TDP-43 per ChAT-positive neurons was less than 80% in confocal analysis (Fig. 2B-b), this is simply because some nucleus are out of vision in the single micrograph depending on the confocal image level. Indeed, almost 100% of ChAT-positive neurons showed nuclear TDP-43 staining by manual observation of confocal microscope. Alternatively, the percentage of TDP-43-positive neurons per Nissl-positive neurons on the ligated side is slightly lower than that on the control side (Fig. 2B-c), which implies the incomplete recovery of ChAT under axonal damage in the mice. These results indicate that redistribution of TDP-43 by axonal ligation correlates with the innervation status and reflect the function of cholinergic neurons.

RNA transcription of TDP-43 is not affected by axonal ligation

To clarify whether aberrant staining of TDP-43 is caused by impaired RNA transcription or by a post-transcrptional event, we performed *in situ* hybridization on day 7 and quantitative real-time PCR analysis of the hypoglossal nucleus using LCM on day 0 and 7 (three mice in each experiment). *In situ* hybridization of TDP-43 revealed that TDP-43 mRNA was equally expressed on the treated side and the control side (Fig. 3A-a). The probe specificity was confirmed by sense probes, which yielded no signal (Fig. 3A-b). We also performed a real-time PCR study to quan-

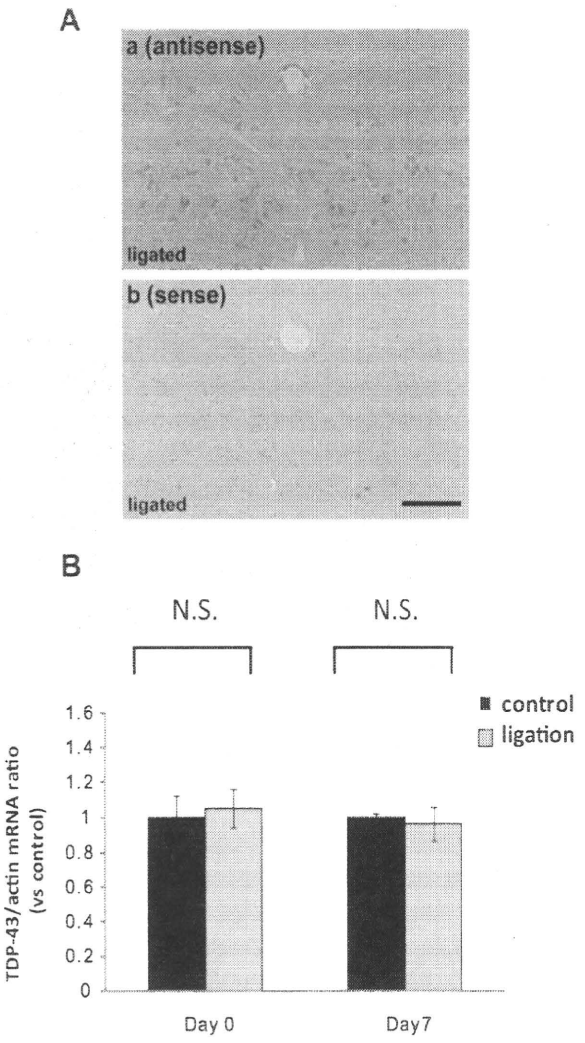

Fig. 3. TDP-43 is not downregulated by axonal ligation, but is excluded from the nucleus (A). In situ hybridization of brainstem slices using antisense (a) or sense (b) probe for TDP-43. There is no difference in the TDP-43 mRNA level between ligated and control sides. The photo is a representative from three mice. Scale bar=200 μm. (B) Quantitative real-time PCR study of TDP-43 and β-actin using cDNA obtained from the isolated hypoglossal nucleus on day 0 and 7 after the ligation using laser capture microdissection. TDP-43/actin mRNA ratio on the ligation side was obtained by comaprtison with the control side, and expressed as fold-increase vs. the control side. There is no trend or statistical significance in the TDP-43 mRNA level between the ligated and control sides (n=3 in each day). N.S., not significant. For interpretation of the references to color in this figure legend, the reader is referred to the Web version of this article.

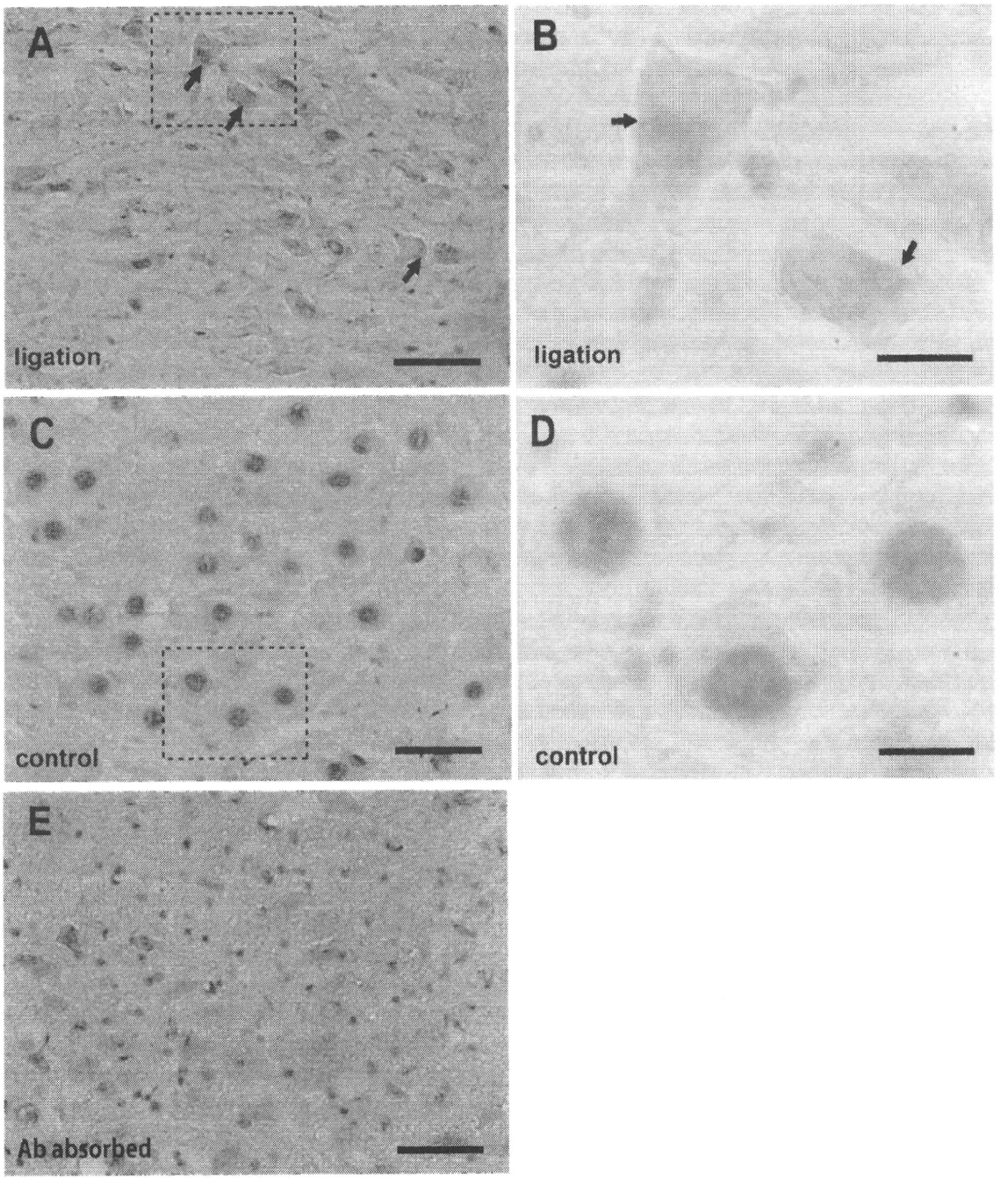

Fig. 4. No involvement carboxyl TDP-43 fragments for cytosolic aggregates in the short term after nerve ligation Immunohistochemistry of brainstem slices subjected to axonal ligation at day 7 with antibodies against the carboxyl terminus of TDP-43. Antibody against the carboxyl terminus of TDP-43 (395–405AA) also showed a similar staining pattern to that against full length or near-amino-terminus of TDP-43. Note that occasional cytosolic TDP-43 was also detected with this antibody (arrows). (A) Bligated side (B, magnified image of demarcated area in A), (C, D) control side (D, magnified image of demarcated area in C). (E) Pre-absorption test at the control side. No immunoreactivity is observed when the antibody was absorbed by antigen peptides (E). Scale bar=100 μm for (A, C, E); 20 μm for (B, D).

tify TDP-43 mRNA in the isolated hypoglossal nucleus subjected to the axonal ligation (three mice). The result shows that the averaged TDP-43 mRNA level, expressed as a value normalized to actin mRNA, was comparable in the treated and untreated sides 7 days after ligation compared with that on day 0 (Fig. 3B), which is in a clear contrast to mRNA change of importin β (Fig. 5C). Our data clearly showed that loss of nuclear staining of TDP-43 is not due to inhibition of gene transcription, but is a nuclear exclusion.

Carboxyl fragments of TDP-43 is not detected in the cytosol at the peak time of nuclear exclusion after nerve ligation

As shown above, we could not detect obvious cytosolic staining of TDP-43 in the neuronal somata on the ligated side using popular rabbit polyclonal antibody (Proteintech) that was raised against full-length recombinant TDP-43. We therefore generated polyclonal rabbit antibody against the carboxyl terminal sequences of TDP-43 (395–414AA)

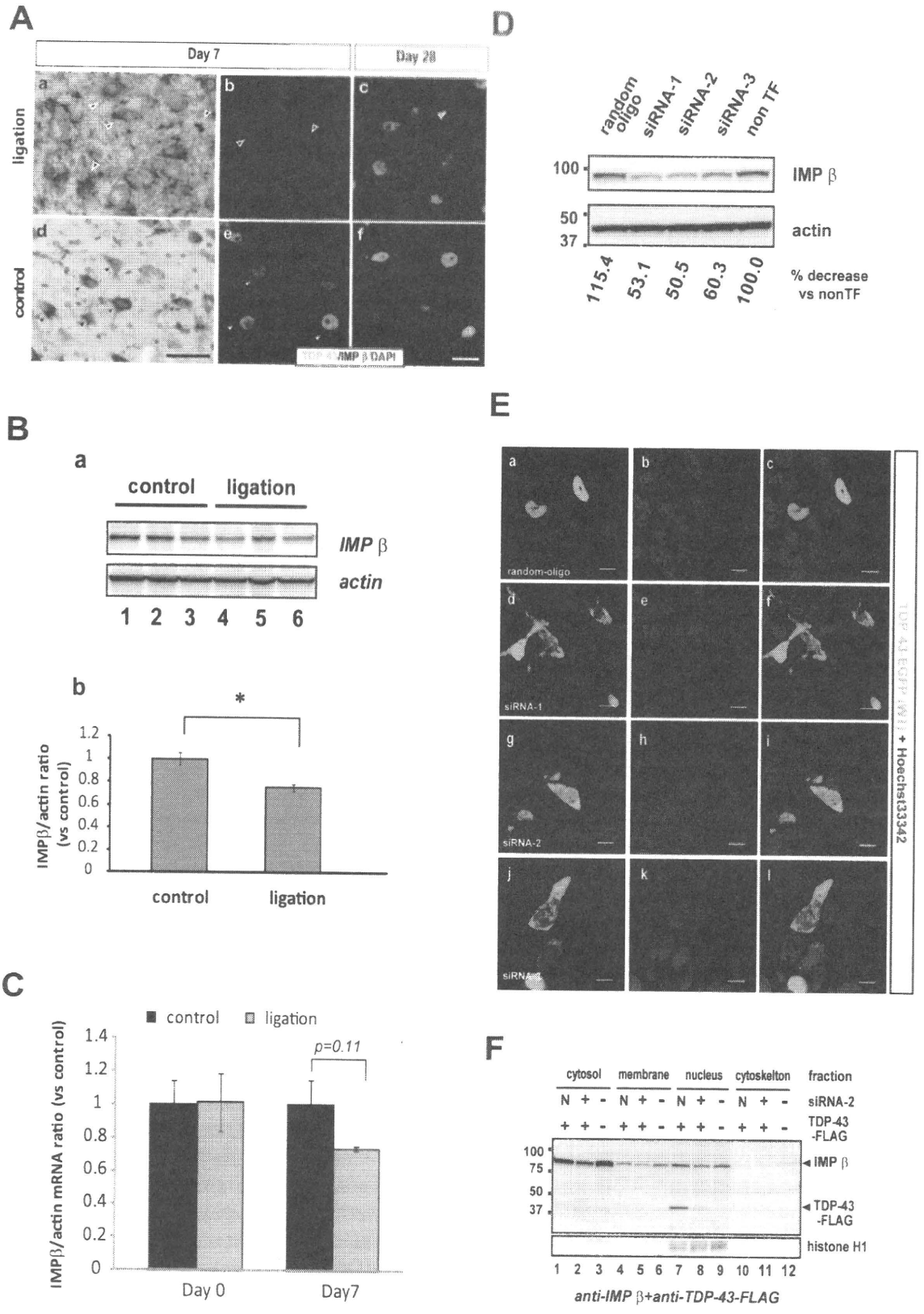

Fig. 5. Transient loss of importing β staining in neuronal somata correlates with aberrant TDP-43 staining after nerve ligation. (A) Immunohistochemistry and immunofluorescence study of brainstem slices for importin β 7 days after hypoglossal ligation. (a, b, d, e) seven days, (c, f) 28 days after ligation. (a, d) Immunostaining using anti-importin β antibody with Nissl counterstain. This antibody labels predominantly cytosolic importin β (arrowheads in d). Importin β staining is reduced in the neuronal somata on the ligated side (a). Scale bar=50 μm. b, c, e, f. Confocal micrographs of brainstem slices double stained with anti-TDP-43 (Proteintech, green) and anti-importin β (red) antibodies. Nuclei were stained by DAPI (blue). b, Weak staining of importin β in the neurons on the ligated side was detected (blanked arrowheads). (e) TDP-43 is normally expressed in the nucleus (arrowheads) surrounded by importin β in the cytoplasm on the untreated side. Scale bar; 200 μm. (c, f) On day 28, both TDP-43 and importin β staining returned to normal (arrows in c). Scale bar=100 μm. Blanked arrowheads indicate endogenous IgG in the active microglia. (B). Western analysis of brainstem hemisections with or without axonal ligation. (a) Western image on the control or the ligation side from three mice 7 days after

to investigate whether fragmented TDP-43 could be observed in the cytosol after axonal ligation, since the carboxyl terminus of TDP-43 has been implicated in cytosolic aggregates, phosphorylation, and ubiquitinated inclusions (Igaz et al., 2009). However, immunostaining with this antibody also showed loss of nuclear TDP-43 with occasional cytosolic staining without overt aggregates (Fig. 4A, B, arrows). The antibody specificity was confirmed by antigen pre-absorption test, in which excess amount of the peptide antigen was preincubated with an antibody before immunoreactions. Preabsorption test successfully eliminated all DAB signals (Fig. 4E). These results indicate that the participation of fragmental TDP-43 in the cytosolic aggregates is not an immediate event to nuclear exclusion.

Nuclear exclusion of TDP-43 correlated to aberrant importin β staining

TDP-43 carries a bipartite nuclear localization signal (NLS; KRKXXXXXXXXXXXXKR), which is recognized by importin α/β. In particular, accumulating evidence has clarified a crucial role of importin β1 in the nuclear transport of most proteins (Pouton et al., 2007). It is reported that the importin β functions in neuronal regeneration upon axonal injury, in which local expression of importin β at the lesion site promotes neuronal survival via facilitating the nuclear transport of cytoprotective molecules such as pErk (Hanz et al., 2003; Perlson et al., 2005). We thus performed immunohistochemistry of importin β in the hypoglossal nucleus after nerve ligation. As shown in Fig. 5A-d, mouse monoclonal antibody detected importin β distributing in the cytosol in the untreated site. Conversely, prominent loss of importin β was observed in the neuronal somata at the ligation site (Fig. 5A-a) compared with the control side. Of note, there is abundant immunoreactivity for importin staining around the hypoglossal somata (Fig. 5A, blanked arrowheads). Since the available antibody against importin β is a mouse monoclonal, the endogenous immunoglobulin in the active microglia on the ligated side, was unavoidably detected (Fig. S1-D). Although we tried to eliminate this background by various blocking protocols, we were unsuccessful. Double immunofluorescent labeling for importin β and TDP-43 (Proteintech) displayed a marked loss of nuclear TDP-43 on the treated side with an accompanied reduction of importin β staining (Fig. 5A-b). This is a clear contrast to the untreated side, which showed co-expression of nuclear TDP-43 and cytosolic importin β (Fig. 5A-e). As observed in ChAT staining, importin β staining on the ligated side returned to the normal pattern 28 days after nerve ligation along with the recovery of TDP-43 (Fig. 5A-c, f). Moreover, Western analysis of the brainstem hemisections revealed that importin β was mildly but significantly reduced compared with the control side (Fig. 5B). Furthermore, the mRNA level for importin β in the hypoglossal nucleus under nerve ligation on day 0 and 7 was also assessed by quantitative real-time PCR using the same protocol as described for TDP-43. Results showed that there was a clear trend of importin β reduction on the ligated side compared with the control side on day 7 and with the same side on day 0 (Fig. 5C), although it was not statistically significant ($P=0.11$ by Student's *t*-test).

To investigate whether importin is involved in the nuclear transport of TDP-43, we studied the knockdown effect of importin β on the nuclear transport of TDP-43 using siRNA in the human neuroblastoma cell-line SHSY-5Y cells. Human neuroblastoma cell-line, SHSY-5Y was transfected with three different siRNA oligonucleotides against importin β, effectively suppressed importin β expression (Fig. 5D). The cells were subsequently transfected with EGFP-fused human TDP-43 for a further 24 h. Confocal laser microscopy revealed that knockdown of importin β resulted in nuclear exclusion of TDP-43 (Fig. 5E). Western analysis of the subcellularly fractionated cell lysates of SHSY-5Y cells that were sequentially transfected with siRNA and TDP-43-FLAG further confirmed the effect of siRNA on the inhibition of nuclear transport of TDP-43 (Fig. 5F). However, we could not conclude a direct interaction between importin β and TDP-43 by *in vitro* binding test because of the weak interaction (not shown). These results agree with recent evidence that redistribution of Ran-GTP, which interacts with importin β in the nucleus for its cytosolic recruitment, prevents the nuclear transport of TDP-43 (Winton et al., 2008).

Peripheral accumulation of TDP-43 after axonal injury with disproportional importin β and impaired axonal autophagy

To further investigate the mechanism of TDP-43 under axonal injury, we analyzed tissue lysates from hypoglossal nerves proximal to the ligation site (Fig. 6A). To our surprise, Western analysis revealed that TDP-43, but not importin β began to accumulate 2 days after the ligation (Fig. 6C, left; 6B, top graph). Although the ratio of TDP-43 or importin β to GAPDH is much higher than to actin on day 2, this is simply because of the transient downregulation of

the unilateral ligation. The blot was incubated with antibodies against importin β and actin. (b) Densitometric analysis showing the significant decrease in importin β/actin ratio by the ligation compared with the control side. $n=3$. * $P<0.05$ by student t. (C) Quantitative real-time PCR assay of importin β in the hypoglossal nucleus. The hypoglossal nucleus was resected from the mice with hypoglossal ligation on day 0 and 7 with laser capture microdissection and cDNA was synthesized from purified total RNA as described in experimental procedures. Importin β/actin mRNA ratio of the ligation side was compared with the control side, and was expressed as fold-increase vs. the control. There is a clear trend showing that ligation inhibits importin β expression, although not statistically significant ($n=3$. $P=0.11$ by student t). (D) Western blotting of total cell lysates from SHSY-5Y cells transfected with siRNA against importin β using anti-importin β and anti-actin antibodies. Three different siRNAs effectively inhibited expression of importin β. The knockdown efficiency in comparison with non-transfection control was indicated in each lane. (E) Confocal laser micrographs. Double-transfected SHSY-5Y cells were fixed with 4% paraformaldehyde after counterstaining with Hoechst33342. Nuclear transport of TDP-43-EGFP was inhibited in the cells carrying three different siRNA (d–f, g–i, j–l) against importin β. Scale bar=100 μm. (F) Western blotting of subcellular fractions from SHSY-5Y cells co-transfected with RNAi (siRNA-2) and TDP-43-FLAG. Cytosolic importin β is effectively diminished leading to loss of nuclear TDP-43 by siRNA (lane 8). N means random control oligomers.

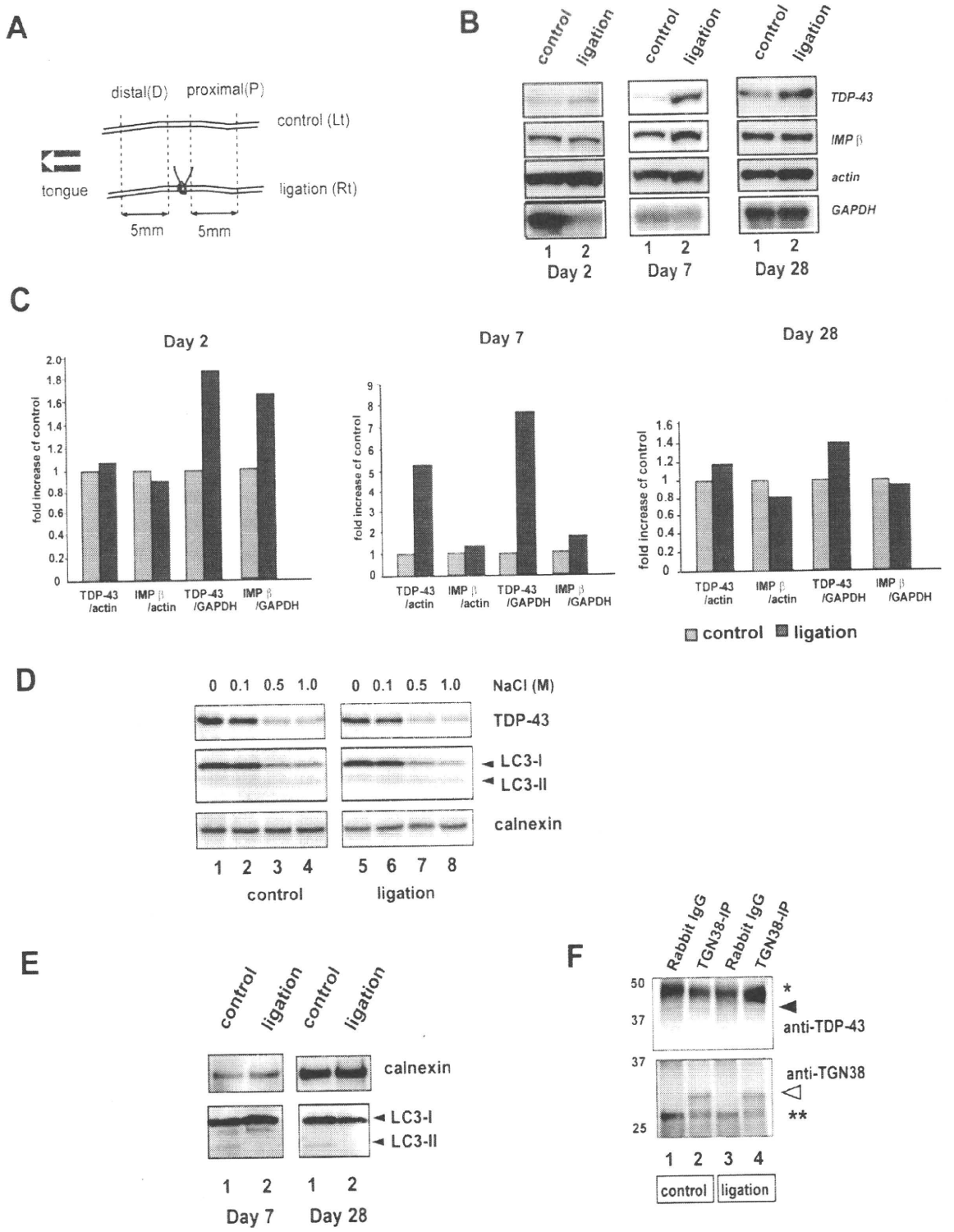

Fig. 6. Western analysis of TDP-43, importin β and active autophagy marker in the hypoglossal nerve subjected to ligation (A) Schematic presentation of the sampling of hypoglossal nerves proximal or distal to the ligation point. Resected hypoglossal nerves were separated into sections 5 mm peripheral and 5 mm central from the ligation point. Three sections from three mice were collected into one tube for Western analysis. (B) Western analysis of resected hypoglossal nerves proximal to the tightening lesion 2, 7 or 28 days after ligation, using antibodies against TDP-43 (Proteintech, top), importin β (2nd), actin (3rd) and GAPDH (bottom). Each lane contains a mixture of nerve lysates from three mice. The TDP-43 blot showed a remarkable increase on day 7 compared with the importin β or actin blot. (C) Densitometric analysis of the immunoblot in B. The value for TDP-43 or importin β was normalized to that of actin or GAPDH. On day 2, the ratio of both TDP-43 and importin β to GAPDH showed a marked increase compared with that to actin. This is due to the transient decrease in GAPDH at this stage under axonal ligation (see Fig. 6B, lane 2 at day 2). Each value was obtained using a pool of nerve pieces of three mice. (D) Hemisection of the brainstem with or without hypoglossal ligation was homogenized and subcellularly fractionated to obtain the microsome fraction as described in the materials and methods (left, control; right, ligation). Western blot using antibodies against TDP-43, LC3 and calnexin after high salt wash experiment of microsome fraction. At the concentration of 0.5–1.0 M NaCl, considerable amount of TDP-43 and LC3-I was released from microsome membranes, while calnexin and LC3-II remains unchanged. A significant amount of TDP-43 is detected in the microsome fraction. (E) Western analysis of the hypoglossal nerves on the ligation and control sides using anti-calnexin or anti-LC3 antibody on day 7 or 28 after ligation. The LC3-II, a marker for active

GAPDH in the acute stage after axonal injury (Fig. 6B lane 2 on the GAPDH blot on day 2, as reported previously; McKerracher, 1993). On day 7, TDP-43, normalized either to actin or to GAPDH, accumulated markedly on the ligated side compared to the control side (Fig. 6B, middle columns, Fig. 6C, middle graph). Importin β was slightly increased despite the declining trend in mRNA in real-time PCR, possibly reflecting regional synthesis of importin ß as reported previously (Hanz et al., 2003). These results imply that an impaired nucleocytoplasmic transport system may underlie the redistribution of TDP-43 after axonal injury.

Since TDP-43 is a nuclear protein and no evidence has been provided as to why TDP-43 can be detected in the peripheral nerves and how it is degraded, we first analyzed the subcellular distribution of TDP-43 in the brainstem hemi-sections. The tissue homogenates were subcellularly fractionated to obtain microsome fractions as described in the Materials and Methods. In the microsome fraction, where the two types of LC3 were present, namely, LC3-I for a cytosolic form and LC3-II for a membrane-bound form (Fig. 6D) as well as an ER marker calnexin, TDP-43 was clearly detected (Fig. 6D, lanes 1 and 5). We further investigated if the TDP-43 in the microsome is intraluminal or membrane-integrated, but not a contaminant from the cytoplasm by a high-salt wash experiment. The microsome fractions were resuspended in 10 mM Tris–HCl buffer with 0, 0.1, 0.5 or 1.0 M NaCl to wash out the contaminant TDP-43 from the cytosol. After a second ultracentrifugation and two washes, the resulting pellets were analyzed with Western blotting using anti-TDP-43, anti-calnexin, and anti-LC3 antibodies. As shown in Fig. 6D, high-salt buffer washed out a considerable amount of TDP-43 and LC3-I by 0.5 M NaCl. However, LC3-II and calnexin, the membrane-integrated proteins remained in the microsome fractions together with a significant amount of TDP-43 even with 1 M NaCl (Fig. 6D, lanes 3, 4, 7, 8). There was no obvious difference between control or ligation side on the expression level of TDP-43, LC3-II, or calnexin in the brainstem hemi-section. We performed Western analysis of the ligated nerves for calnexin and LC3, and found that the ligation markedly decreased in LC3-II with a concomitant increase in LC3-I on day 7, indicating that active autophagosome is impaired in the peripheral axon (Figs. 6E-a, b). Conversely, calnexin showed a slight increased by the ligation. These data indicated that TDP-43, transported in the axonal flow, was constitutively cleared by autophagy (Urushitani et al., 2009), and that the autophagy dysfunction under axonal damage might be associated with peripheral accumulation of TDP-43. Finally, to test the possibility that TDP-43 is carried via trans-Golgi network, we performed immunoblotting using anti-TDP-43 antibody using immunoisolated TGN from brainstem hemi-sections (Urushitani et al., 2006). However, TDP-43 was not present in the TGN vesicles (Fig. 6F).

DISCUSSION

In this report, we showed that axonal ligation induced transient nuclear exclusion of TDP-43 in hypoglossal neurons. The aberrant TDP-43 staining correlated with the ChAT immunoreactivity, indicative of the link between the subcellular localization of TDP-43 and axonal degeneration/regeneration. Redistribution of TDP-43 was a post-translational event since the levels of mRNA of TDP-43 were not affected by the ligation as shown in quantitative real-time PCR and *in situ* hybridization. We also demonstrated that axonal ligation induced aberrant localization of importin β and defect in active autophagosome, which accounts for the accumulation of TDP-43 on the injured axon. Together with our recent finding, showing that TDP-43 is predominantly decayed in the autophagosomes (Urushitani et al., 2009), these results explain the missing link between axonal damage and the redistribution of TDP-43 as observed by Moisse et al (Moisse et al., 2009) and us. However, there are several significant differences between their report and the present study. In their report, there is an upregulation of TDP-43 by axotomy, whereas we found no difference in the case of axonal ligation. The population of motor neurons with nuclear excluded TDP-43 in this paper was less than that in our study. The possible reasons to explain several discrepancies may include (1) a surgery strategy, namely axotomy or axonal ligation, (2) the nerves used for the study; hypoglossal nerve or sciatic nerve, and (3) the sample preparation for mRNA quantification. First, we studied the effect of axotomy as well as axonal ligation on the TDP-43 redistribution, and found that axotomy induced nuclear exclusion to a lesser extent than axonal ligation (Fig. S2). Our guess to explain the difference between the two is that the axonal ligation leads to higher accumulation of the transported molecules than axotomy does. Second, the hypoglossal nerve is a pure motor neuron, while the sciatic nerve contains both motor and sensory neurons, the axotomy of which may induce the different regulation of TDP-43. Finally, for mRNA quantification, we isolated hypoglossal nucleus using laser capture microdissection, while they used hemi-spinal cord that contains abundant non-motor cells. It is possible that gliosis induced by axotomy contributed to the result of mRNA level of TDP-43 in the hemi-spinal cord. Indeed, we also observed robust microgliosis and astrogliosis on day 7 after ligation (Fig. S1, C, D). Further investigation of molecular machineries under different injury types and neuron types may contribute to uncover the mechanism of redistribution of TDP-43. It should be noted however, it is technically difficult to precisely adjust the quantity of mRNA

autophagosomes was absent in the operated nerves in both day 7 and 28. (F) TDP-43 is not present in the trans-Golgi network. The supernatant excluding mitochondrial fraction after 10,000 g×5 min, was immunoprecipitated with anti-TGN38 antibody which had been cross-linked to Protein G-magnet beads. The immunoprecipitates were eluted and analyzed by Western blotting using anti-TDP-43 (top) or anti-TGN38 antibody. There was no significant bad for TDP-43 showing it presence in the TGN. Each lane or value was obtained from the pooled tissue lysates from three mice. The ligation experiments were repeated at least twice, and the representative data were presented.

from hypoglossal neurons by LCM, and actin mRNA was slightly elevated on the ligation side. Therefore, we cannot exclude the possibility that mRNA is upregulated in the neurons at the ligation side as reported by Moisse et al. However, in *situ* hybridization verified that there is no obvious difference between the control and the operation side. Most importantly, our results indicate that the transient nuclear loss of TDP-43 was not caused by its downregulation.

The impact of TDP-43 redistribution in the pathogenesis of ALS

Despite the marked nuclear exclusion of TDP-43 after the axonal ligation, transient loss of nuclear TDP-43 was not lethal to motor neurons. This finding indicates that redistribution itself, at least in a period of short term, is not a trigger for motor neuron death. This result is consistent with the previous report using sciatic nerve (Moisse et al., 2009). However, if sequestration of TDP-43 perpetually affects normal TDP-43 function, it might cause neurotoxicity as shown in a siRNA study (Ayala et al., 2008). We also investigated another cholinergic neuron, the dorsal nucleus of vagus, which projects efferent autonomic nerves to the intestines. The results showed a similar redistribution of TDP-43 in the dorsal nucleus of vagus (Fig. S3, A–D), indicating that nuclear exclusion of TDP-43 under axonal damage was not limited to motor neurons. Of note, increasing lines of evidence have shown that TDP-43 pathology is detected not only in FTLD-U or ALS but also in Pick disease (Freeman et al., 2008), Lewy body disease (Nakashima-Yasuda et al., 2007), hippocampal sclerosis and even in Alzheimer's disease (Amador-Ortiz et al., 2007), suggesting that TDP-43 pathology is shared in downstream cascades in a broad spectrum of neurological diseases.

Interestingly, restoration of TDP-43 is tightly associated with ChAT expression. Pathophysiological significance of the recovery of ChAT staining in the chronic stage after nerve injury is not fully understood. However, Bussmann and Sofroniew (1999) substantiated that loss of ChAT expression is caused by disruption of retrograde axonal signal, using the various axonal injuries. It is also reported that expression of vesicular choline acetyltransferase (VAChT), a cholinergic marker at the nerve terminal correlates with the regeneration of neuro-muscular junction, using anterograde or retrograde tracers (Maeda et al., 2004). Therefore, it is conceivable that restoration of nuclear TDP-43 may reflect axonal regeneration, which is indicated by ChAT upregulation. Although we have no clear answer to explain why TDP-43 is partially affected, one possible explanation would be that hemi-lesion affects the function of contralateral hypoglossal nucleus mediated by commissural axons connecting both hypoglossal nucleus (Tarras-Wahlberg and Rekling, 2009). In agreement with this idea, ChAT staining on day 7 and 14 was partially reduced on the unlesioned contralateral side as shown in Fig. 1A.

Unexpectedly, regardless of the marked elimination of nuclear TDP-43, no typical aggregates were observed in the neuronal somata. Carboxyl fragment accumulation is unlikely since our antibody raised against carboxyl terminus (395–414 AA) of TDP-43 demonstrated no aggregates. This result indicates that fragment accumulation of TDP-43 is time-consuming and a more downstream event after the neurotoxic pathway commences. Another possibility might be that nuclear excluded TDP-43 is transported by axonal flow as shown in this report. It is also possible that nucleus-excluded TDP-43 is rapidly cleared at proteasomes or in the autophagy-lysosome system in the soma as discussed below.

Importin β and nuclear localization of TDP-43

Our study suggests that insufficient expression or altered distribution of importin β under axonal ligation is associated with mislocalization of TDP-43. At 7 days after nerve ligation, there was a trend in which importin β mRNA expression in the ligated side was reduced compared with the untreated side, and immunostaining for importin β showed a marked decrease in the cytosol. Conversely, Western analysis displayed mild accumulation of importin β in the peripheral nerves proximal to the ligation site (1.34-fold vs. unlesioned side), followed by recovery in both the cytosol and peripheral nerve at 28 days after ligation. Since the accumulation of TDP-43 is extremely high (5.29-fold higher), this might have overwhelmed expression level of importin β for proper translocation of TDP-43 to the nucleus. Further evidence is required to conclude that importin β is centrally involved in TDP-43 mislocalization after axonal ligation. Nevertheless, a siRNA study against importin β using a transfected cell-line clearly indicates that nuclear transport of TDP-43 is importin β-dependent. This is consistent with previous reports describing that nuclear localization of TDP-43 is severely affected by the mislocalization of Ran-GTP, a partner with importin β in the nucleocytoplasmic transport system (Winton et al., 2008). In the light of recent evidence that importin β is involved in axonal regeneration after peripheral injury to prioritize the nuclear import of pro-survival transcription factors such as p-Erks (Hanz et al., 2003), we speculate that TDP-43 is not ranked high in emergent condition such as axonal injury in the process of axonal regeneration.

TDP-43 in the axon

To our surprise, there was a marked accumulation of TDP-43 in the proximal section to the tightened site. By observing the coronal section of the hypoglossal nerves proximal to the ligation, we confirmed that there is no cell proliferation around the analyzed nerve pieces (Fig. S4), so the accumulation of TDP-43 is an event inside the hypoglossal nerves. We also showed that increase in TDP-43 correlated to decrease in LC3-II, a marker for active autophagosomes under the axonal ligation. Therefore, TDP-43 in the peripheral axon might accumulate because of defective active autophagosome, as well as importin disproportion. A considerable amount of TDP-43 still accumulated, whereas nuclear TDP-43 restored on day 28 (Fig. 6E). This can be reasoned by the local defect

in autophagosomes suffering the axonal ligation. This finding fits the recent notion that an inhibitor of autophagy induced cytosolic aggregates of TDP-43 (Kim et al., 2008; Urushitani et al., 2009). Alternatively, the possibility that TDP-43 distributed with ER in the axon cannot be excluded. Although ultrastructural analysis suggests that axons do not have rough ER, recent paper documented ER components for local protein synthesis in the peripheral axon (Merianda et al., 2009). Considering the fact that neurofilament synthesis is regionally regulated in peripheral axons (Sotelo-Silveira et al., 2000), TDP-43 might form the complex with the ER for the protein synthesis of neurofilament L. This notion agrees with the previous finding that TDP-43 interacts with the mRNA of low molecular neurofilament (NFL) (Strong et al., 2007). Then, it is tempting to hypothesize that microsomal TDP-43 may explain a previous paper describing that TDP-43 is detected in the cerebrospinal fluid of ALS patients (Steinacker et al., 2008). However, we found that TDP-43 is not present in the trans-Golgi network, indicating that TDP-43 is not present in the post-Golgi transport vesicles.

CONCLUSION

In conclusion, our results revealed that axonal flow damage is associated with the redistribution of TDP-43 through the combined effects of defective axonal autophagic clearance and impaired importing system. These results provide huge insights to understand the mechanisms of TDP-43 accumulations in ALS. There are still many missing links between TDP-43 redistribution and axonal flow damage yet to be clarified. Further investigation of the molecular machineries of nuclear exclusion of TDP-43 will be helpful in both an understanding of and therapeutic development against ALS.

Acknowledgments—We thank Drs. T. Hattori and H. Sugihara at department of pathology of Shiga University of Medical Science (SUMS) for their generous permission to use the laser capture microdissection system, and we thank T. Nakayama for his technical help. We thank T. Yamamoto in the central research laboratory at SUMS for his technical help in confocal laser microscope experiment. The experimental help by H. Kita and R. Ohtake is thankfully acknowledged. This work is supported by research grant from Japan Society of Promotion of Science (JSPS), Japan Health and Labour Science Research Grants, Japan ALS Association, Takeda Science Foundation and Presidential Grant-in-Aid from SUMS.

REFERENCES

Amador-Ortiz C, Lin WL, Ahmed Z, Personett D, Davies P, Duara R, Graff-Radford NR, Hutton ML, Dickson DW (2007) TDP-43 immunoreactivity in hippocampal sclerosis and Alzheimer's disease. Ann Neurol 61:435–445.

Arai T, Hasegawa M, Akiyama H, Ikeda K, Nonaka T, Mori H, Mann D, Tsuchiya K, Yoshida M, Hashizume Y, Oda T (2006) TDP-43 is a component of ubiquitin-positive tau-negative inclusions in frontotemporal lobar degeneration and amyotrophic lateral sclerosis. Biochem Biophys Res Commun 351:602–611.

Ayala YM, Misteli T, Baralle FE (2008) TDP-43 regulates retinoblastoma protein phosphorylation through the repression of cyclin-dependent kinase 6 expression. Proc Natl Acad Sci U S A 105:3785–3789.

Bussmann KA, Sofroniew MV (1999) Re-expression of p75NTR by adult motor neurons after axotomy is triggered by retrograde transport of a positive signal from axons regrowing through damaged or denervated peripheral nerve tissue. Neuroscience 91:273–281.

Dickson DW, Josephs KA, Amador-Ortiz C (2007) TDP-43 in differential diagnosis of motor neuron disorders. Acta Neuropathol (Berl) 114:71–79.

Freeman SH, Spires-Jones T, Hyman BT, Growdon JH, Frosch MP (2008) TAR-DNA Binding Protein 43 in Pick Disease. J Neuropathol Exp Neurol 67:62–67.

Gitcho MA, Baloh RH, Chakraverty S, Mayo K, Norton JB, Levitch D, Hatanpaa KJ, White CL III, Bigio EH, Caselli R, Baker M, Al-Lozi MT, Morris JC, Pestronk A, Rademakers R, Goate AM, Cairns NJ (2008) TDP-43 A315T mutation in familial motor neuron disease. Ann Neurol 63:535–538.

Hanz S, Perlson E, Willis D, Zheng JQ, Massarwa R, Huerta JJ, Koltzenburg M, Kohler M, van-Minnen J, Twiss JL, Fainzilber M (2003) Axoplasmic importins enable retrograde injury signaling in lesioned nerve. Neuron 40:1095–1104.

Igaz LM, Kwong LK, Chen-Plotkin A, Winton MJ, Unger TL, Xu Y, Neumann M, Trojanowski JQ, Lee VM (2009) Expression of TDP-43 C-terminal fragments in vitro recapitulates pathological features of TDP-43 proteinopathies. J Biol Chem 284:8516–8526.

Julien JP (2001) Amyotrophic lateral sclerosis. Unfolding the toxicity of the misfolded. Cell 104:581–591.

Kabashi E, Valdmanis PN, Dion P, Spiegelman D, McConkey BJ, Velde CV, Bouchard JP, Lacomblez L, Pochigaeva K, Salachas F, Pradat PF, Camu W, Meininger V, Dupre N, Rouleau GA (2008) TARDBP mutations in individuals with sporadic and familial amyotrophic lateral sclerosis. Nat Genet 40:572–574.

Kim SH, Shi Y, Hanson KA, Williams LM, Sakasai R, Bowler MJ, Tibbetts RS (2008) Potentiation of ALS-associated TDP-43 aggregation by the proteasome-targeting factor, Ubiquilin 1. J Biol Chem 284:8083–8092.

Kwong LK, Neumann M, Sampathu DM, Lee VM, Trojanowski JQ (2007) TDP-43 proteinopathy: the neuropathology underlying major forms of sporadic and familial frontotemporal lobar degeneration and motor neuron disease. Acta Neuropathol (Berl) 114:63–70.

Lams BE, Isacson O, Sofroniew MV (1988) Loss of transmitter-associated enzyme staining following axotomy does not indicate death of brainstem cholinergic neurons. Brain Res 475:401–406.

Lee EB, Lee VM, Trojanowski JQ, Neumann M (2008) TDP-43 immunoreactivity in anoxic, ischemic and neoplastic lesions of the central nervous system. Acta Neuropathol (Berl) 115:305–311.

Maeda M, Ohba N, Nakagomi S, Suzuki Y, Kiryu-Seo S, Namikawa K, Kondoh W, Tanaka A, Kiyama H (2004) Vesicular acetylcholine transporter can be a morphological marker for the reinnervation to muscle of regenerating motor axons. Neurosci Res 48:305–314.

Matsuura J, Ajiki K, Ichikawa T, Misawa H (1997) Changes of expression levels of choline acetyltransferase and vesicular acetylcholine transporter mRNAs after transection of the hypoglossal nerve in adult rats. Neurosci Lett 236:95–98.

McKerracher L, Essagian C, Aguayo AJ (1993) Marked increase in beta-tubulin mRNA expression during regeneration of axotomized retinal ganglion cells in adult mammals. J Neurosci 13:5294–5300.

Merianda TT, Lin AC, Lam JS, Vuppalanchi D, Willis DE, Karin N, Holt CE, Twiss JL (2009) A functional equivalent of endoplasmic reticulum and Golgi in axons for secretion of locally synthesized proteins. Mol Cell Neurosci 40:128–142.

Moisse K, Volkening K, Leystra-Lantz C, Welch I, Hill T, Strong MJ (2009) Divergent patterns of cytosolic TDP-43 and neuronal progranulin expression following axotomy: implications for TDP-43 in the physiological response to neuronal injury. Brain Res 1249: 202–211.

Nakashima-Yasuda H, Uryu K, Robinson J, Xie SX, Hurtig H, Duda JE, Arnold SE, Siderowf A, Grossman M, Leverenz JB, Woltjer R, Lopez OL, Hamilton R, Tsuang DW, Galasko D, Masliah E, Kaye J, Clark CM, Montine TJ, Lee VM, Trojanowski JQ (2007) Co-morbidity of TDP-43 proteinopathy in Lewy body related diseases. Acta Neuropathol (Berl) 114:221–229.

Neumann M, Sampathu DM, Kwong LK, Truax AC, Micsenyi MC, Chou TT, Bruce J, Schuck T, Grossman M, Clark CM, McCluskey LF, Miller BL, Masliah E, Mackenzie IR, Feldman H, Feiden W, Kretzschmar HA, Trojanowski JQ, Lee VM (2006) Ubiquitinated TDP-43 in frontotemporal lobar degeneration and amyotrophic lateral sclerosis. Science 314:130–133.

Nonaka T, Arai T, Buratti E, Baralle FE, Akiyama H, Hasegawa M (2009) Phosphorylated and ubiquitinated TDP-43 pathological inclusions in ALS and FTLD-U are recapitulated in SH-SY5Y cells. FEBS Lett 583:394–400.

Otis KO, Thompson KR, Martin KC (2006) Importin-mediated nuclear transport in neurons. Curr Opin Neurobiol 16:329–335.

Perlson E, Hanz S, Ben-Yaakov K, Segal-Ruder Y, Seger R, Fainzilber M (2005) Vimentin-dependent spatial translocation of an activated MAP kinase in injured nerve. Neuron 45:715–726.

Pouton CW, Wagstaff KM, Roth DM, Moseley GW, Jans DA (2007) Targeted delivery to the nucleus. Adv Drug Deliv Rev 59:698–717.

Sotelo-Silveira JR, Calliari A, Kun A, Benech JC, Sanguinetti C, Chalar C, Sotelo JR (2000) Neurofilament mRNAs are present and translated in the normal and severed sciatic nerve. J Neurosci Res 62:65–74.

Sreedharan J, Blair IP, Tripathi VB, Hu X, Vance C, Rogelj B, Ackerley S, Durnall JC, Williams KL, Buratti E, Baralle F, de Belleroche J, Mitchell JD, Leigh PN, Al-Chalabi A, Miller CC, Nicholson G, Shaw CE (2008) TDP-43 mutations in familial and sporadic amyotrophic lateral sclerosis. Science 319:1668–1672.

Steinacker P, Hendrich C, Sperfeld AD, Jesse S, von Arnim CA, Lehnert S, Pabst A, Uttner I, Tumani H, Lee VM, Trojanowski JQ, Kretzschmar HA, Ludolph A, Neumann M, Otto M (2008) TDP-43 in cerebrospinal fluid of patients with frontotemporal lobar degeneration and amyotrophic lateral sclerosis. Arch Neurol 65:1481–1487.

Strong MJ, Volkening K, Hammond R, Yang W, Strong W, Leystra-Lantz C, Shoesmith C (2007) TDP43 is a human low molecular weight neurofilament (hNFL) mRNA-binding protein. Mol Cell Neurosci 35:320–327.

Tarras-Wahlberg S, Rekling JC (2009) Hypoglossal motoneurons in newborn mice receive respiratory drive from both sides of the medulla. Neuroscience 161:259–268.

Urushitani M, Sato M, Bamba H, Hisa Y, Tooyama I (2009) Synergistic effect between proteasome and autophagosome in the clearance of poly-ubiquitinated TDP-43. J Neurosci Res; doi:10.1002/jnr.22243.

Urushitani M, Sik A, Sakurai T, Nukina N, Takahashi R, Julien JP (2006) Chromogranin-mediated secretion of mutant superoxide dismutase proteins linked to amyotrophic lateral sclerosis. Nat Neurosci 9:108–118.

Winton MJ, Igaz LM, Wong MM, Kwong LK, Trojanowski JQ, Lee VM (2008) Disturbance of nuclear and cytoplasmic Tar DNA binding protein (TDP-43) induces disease-like redistribution, sequestration and aggregate formation. J Biol Chem 283:13302–13309.

Yokoseki A, Shiga A, Tan CF, Tagawa A, Kaneko H, Koyama A, Eguchi H, Tsujino A, Ikeuchi T, Kakita A, Okamoto K, Nishizawa M, Takahashi H, Onodera O (2008) TDP-43 mutation in familial amyotrophic lateral sclerosis. Ann Neurol 63:538–542.

Zhang YJ, Xu YF, Dickey CA, Buratti E, Baralle F, Bailey R, Pickering-Brown S, Dickson D, Petrucelli L (2007) Progranulin mediates caspase-dependent cleavage of TAR DNA binding protein-43. J Neurosci 27:10530–10534.

APPENDIX

Supplementary data

Supplementary data associated with this article can be found, in the online version, at doi:10.1016/j.neuroscience.2009.09.050.

(Accepted 19 September 2009)
(Available online 25 September 2009)

J Neuropathol Exp Neurol

Vol. 69, No. 10
October 2010
pp. 1044–1056

ORIGINAL ARTICLE

Induction of Protective Immunity by Vaccination With Wild-Type Apo Superoxide Dismutase 1 in Mutant SOD1 Transgenic Mice

Shigeko Takeuchi, MS, Noriko Fujiwara, PhD, Akemi Ido, PhD, Miki Oono, MD, Yuki Takeuchi, MD, Minako Tateno, PhD, Keiichiro Suzuki, MD, PhD, Ryosuke Takahashi, MD, PhD, Ikuo Tooyama, MD, PhD, Naoyuki Taniguchi, MD, PhD, Jean-Pierre Julien, PhD, and Makoto Urushitani, MD, PhD

Abstract

Vaccinations targeting extracellular superoxide dismutase 1 (SOD1) mutants are beneficial in mouse models of amyotrophic lateral sclerosis (ALS). Because of its misfolded nature, wild-type nonmetallated SOD1 protein (WT-apo) may have therapeutic application for vaccination of various SOD1 mutants. We compared the effects of WT-apo to those of a G93A SOD1 vaccine in low-copy G93A SOD1 transgenic mice. Both SOD1 vaccines induced antibody against G93A SOD1 and significantly delayed disease onset compared with saline/adjuvant controls. WT-apo SOD1 significantly extended the life span of vaccinated mice. The vaccines potentiated T_H2 deviation in the spinal cord as determined by the ratio of interleukin-4 to interferon-γ (IFNγ) or tumor necrosis factor and induced C1q deposition around motor neurons. Transgenic mice had abundant microglial expression of signal transducers and activators of transcription 4, an activator of transcription of IFNγ, in the spinal cord implicating IFNγ in the pathogenesis. On the other hand, the sera from G93A SOD1-vaccinated mice showed higher IFNγ or tumor necrosis factor and yielded a lower IgG1/IgG2c ratio than the sera from WT-apo–vaccinated mice. These results indicate that the T_H1/T_H2 milieu is affected by specific vaccinations and that antigenicity might counteract beneficial effects by enhancing T_H1 immunity. Thus, because of its lower T_H1 induction, WT-apo may be a therapeutic option and have broader application in ALS associated with diverse SOD1 mutations.

Key Words: Acquired immunity, Amyotrophic lateral sclerosis, Superoxide dismutase 1, Transgenic mice, Vaccination.

INTRODUCTION

Amyotrophic lateral sclerosis (ALS) is a lethal neurodegenerative disease characterized by progressive muscle weakness and wasting. Although the precise pathogenetic mechanisms of ALS remain elusive, diverse genetic mutations have been identified in familial ALS cases and are risk factors for both sporadic and familial ALS (1). Mutations in superoxide dismutase 1 (SOD1) account for 20% of familial ALS and have been determined to be the cause of motor neuron degeneration in many instances (2). Moreover, transgenic (Tg) mice carrying the human SOD1 mutation represent an excellent animal model of ALS (3). Importantly, the concept of non–cell-autonomous motor neuron death was derived from intensive analyses of mutant SOD1 Tg mice, which has had a major impact on understanding and treating not only mutant SOD1-linked ALS but also other neurodegenerative diseases such as Parkinson, Alzheimer, and Huntington diseases (4–6). There is also growing interest in the hypothesis of prion-like spreading of disease-causing proteins in such diseases (7, 8).

On the basis of our findings that chromogranin A/B may act as chaperone-like proteins to promote secretion of mutant SOD1 (9), we targeted extracellular SOD1 of G37R SOD1 Tg mice using a G93A mutant SOD1 vaccine, which resulted in a significant delay in disease onset and extension of the life span of the vaccinated mice (10). However, vaccination against high-copy G93A SOD1 (G93AGur) mice was not effective. We ascribed this failure to the extremely high expression level of the transgene. It is also possible, however, that a combination of specific antigen and the host immune response can counteract the beneficial effects of vaccination. For example, in a report testing amyloid-β (Aβ) vaccines of wild-type (WT) or various mutations linked to familial Alzheimer disease, different inflammatory responses and IgG subclasses were elicited depending on the type of Aβ vaccine used; antibody titer against Aβ in each vaccine was high overall (11). Another approach by Kutzler et al (12) using DNA vaccines encoding WT or Flemish/Dutch mutant Aβ showed greater antigenicity

From the Molecular Neuroscience Research Center (ST, AI, MO, IT, MU), Shiga University of Medical Science, Shiga; Department of Biochemistry (NF, YT, KS), Hyogo College of Medicine, Hyogo; Department of Peripheral Nervous System Research (MT), National Institute of Neuroscience, National Center of Neurology and Psychiatry, Tokyo, Japan; Department of Psychiatry and Neuroscience (J-PJ), Research Centre of CHUQ, Laval University, Quebec, Canada; Department of Disease Glycomics (Seikagaku Corporation) (NT), The Institute of Scientific and Industrial Research, Osaka University, Osaka; Systems Glycobiology Group (NT), Disease Glycomics Team, Advanced Science Institute, RIKEN, Saitama; and Department of Neurology (MO, RT), Kyoto University, Kyoto, Japan.

Send correspondence and reprint requests to: Makoto Urushitani, MD, PhD, Unit for Neurobiology and Therapeutics, Molecular Neuroscience Research Center, Shiga University of Medical Science; Shiga, Japan; E-mail: uru@belle.shiga-med.ac.jp

This study was funded by the Japan Society for the Promotion of Science, Japan Health and Labour Science Research Grants, Japan ALS Association, and Takeda Science Foundation.

Supplemental digital content is available for this article. Direct URL citations appear in the printed text and are provided in the HTML and PDF versions of this article on the journal's Web site (www.jneuropath.com).

and T_H1 immune response to the mutant than the WT Aβ peptide. The T_H1 cytokines tumor necrosis factor (TNF) and interferon-γ (IFNγ) are implicated in motor neuron degeneration in ALS (13, 14), whereas the T_H2 cytokine interleukin-4 (IL-4) provides protective immunity to prevent motor neuron death (15). Moreover, T cells are present in the spinal cord of ALS patients (16), and circulating $CD4^+$ T cells affect the disease course of ALS model mice (17–19). In particular, $CD4^+$ T cells stimulate astrocytes or microglia to express neuroprotective molecules including glutamate transporter or insulin-like growth factor 1 (IGF-1) (17). The effects of different types of acquired immunity induced by different vaccines on the therapeutic outcome, however, have not been systematically studied.

More than 120 mutations in SOD1 covering overall domains have been reported. Therefore, it would be desirable to develop a vaccine that is effective and not dependent on thespecific SOD1 mutation associated with the disorder. One approach is to target the core domain of the molecule, i.e. the dimer interface (20). Another approach is to use apo WT SOD1, the molecular behavior of which is similar to that of the mutant molecules (21, 22). We previously reported that wild-type (WT) SOD1 with posttranslational modifications, including oxidative modification, gains properties similar to those of mutant SOD1 (10). Other reports show possible involvement of WT SOD1 in the pathogenesis of sporadic ALS. For example WT SOD1 has been detected in cytoplasmic aggregates and abnormal dimer formations have been reported in the spinal cord of sporadic ALS patients (23, 24). Therefore, the development of SOD1 vaccine based on the WT sequence deserves investigation because of its potential broad application not only in mutant SOD1-associated but also in sporadic ALS.

Here, we compared the effects of G93A-apo SOD1 and WT-apo SOD1 vaccines on the survival and the life span of low-copy G93A SOD1 Tg mice ($G93AGur^{dl}$) and analyzed the relationships to the cellular and humoral immune responses elicited by the vaccinations.

MATERIALS AND METHODS

Materials

All chemicals were obtained from Nacalai Tesque, Inc (Kyoto, Japan), unless specified otherwise, and were of the highest grade available.

Purification of Recombinant SOD1 From *Escherichia coli*

Recombinant human WT and gly93ala (G93A) mutant SOD1 were produced in *Escherichia coli* according to a previous report (22). The eluates were dialyzed against endotoxin-free saline and subsequently stored at −80°C until use. Metallation of the recombinant SOD1 was performed as previously described (22). The metallated and nonmetallated SOD1s were designated as holo-SOD1s and apo-SOD1s, respectively. Control monomeric SOD1 was prepared by treating recombinant human SOD1 chemically modified with 2-mercaptoethanol at Cys111 (2-ME-SOD1 (25). The purity of the recombinant protein was assessed by sodium dodecyl sulfate-polyacrylamide gel electrophoresis (SDS-PAGE) and gel staining with Coomassie brilliant blue. Details are provided in Methods, Supplemental Digital Content 1, http://links.lww.com/NEN/A178.

Molecular-Size Filtration Chromatography

A total of 100 μL of SOD1 proteins (2–3 mg/mL) in phosphate-buffered saline (PBS) (−) were applied to a molecular-size filtration high-performance liquid chromatography (AKTA Explorer 10S) at a flow rate of 0.5 mL/min on Superdex 75 10/30 (GE Healthcare, Piscataway, NJ) equilibrated with 50 mmol/L sodium phosphate buffer containing 0.15 mol/L NaCl, pH 7.4. The calibration of the column for the estimation of molecular weight was performed using bovine serum albumin (Intergen, Milford, MA), ovalbumin (GE Healthcare), and *E. coli* thioredoxin (Promega, Madison, WI), as protein standards.

Animal Experiments

Tg mice harboring human G93A SOD1 (B6SJL-TgN[SOD1-G93A]1Gur, hSOD1G93A; Jackson Laboratory, Bar Harbor, ME) were backcrossed with C57BL/6 strain for more than 20 generations ($G93AGur^{dl}$). $G93AGur^{dl}$ mice were vaccinated with apo recombinant human SOD1 (WT or G93A) or human erythrocyte-derived SOD1 (Sigma) with Monophosphoryl Lipid A- Trehalose Dicorynomycolate (MPL-TDM; Ribi) adjuvant, as previously reported (10). From day 100, motor performance was evaluated for onset of decreased rotarod retention time (Muromachi, Tokyo, Japan) and body weight (BW) change to determine the time of onset (Methods, Supplemental Digital Content 1, http://links.lww.com/NEN/A178). The data for the survival and onset were analyzed by Kaplan-Meyer curve and log-rank test using Prism software (GraphPad, La Jolla, CA).

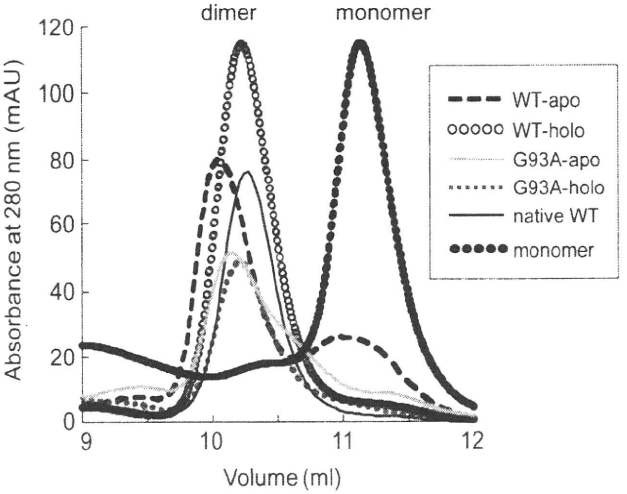

FIGURE 1. Characterization of recombinant human G93A or wild-type (WT)-apo superoxide dismutase 1 (SOD1) proteins. The chromatogram profile of SOD1 proteins separated with a gel filtration column. The native WT-SOD1, apo-WT, apo-G93A, holo-WT, holo-G93A, and monomeric SOD1, were eluted on Superdex 75 column. The elution profiles were monitored by the absorbance change at 280 nm. apo- indicates nonmetallated; holo-, metallated.

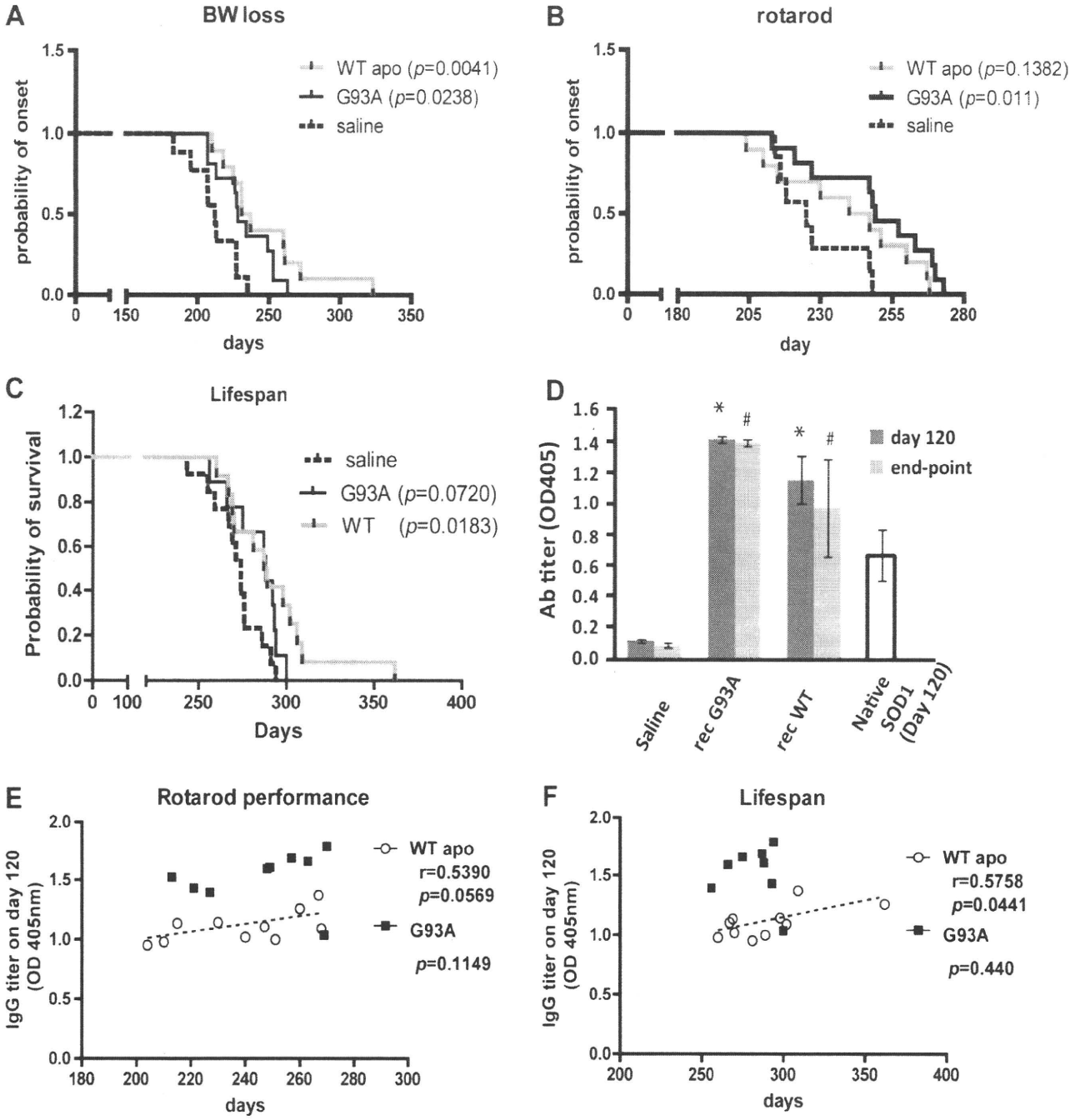

FIGURE 2. Effects of vaccination with recombinant human G93A-apo or wild-type (WT)-apo superoxide dismutase 1 (SOD1) proteins on clinical disease and antibody (Ab) responses in low-copy G93A SOD1 Tg mice (G93AGur^{dl}). **(A, B)** Both the G93A-apo and the WT-apo vaccines significantly delayed the disease onset of G93AGur^{dl} mice. Time of the onset was determined based on body weight (BW) loss **(A)** and impaired rotarod performance **(B)**. **(C)** The WT-apo SOD1 vaccine significantly extended the life span of G93AGur^{dl} mice; the G93A-apo SOD1 vaccine showed a nonsignificant trend. $p < 0.05$ by Kaplan-Meyer curve and log-rank test; n = 13 for saline/adjuvant, n = 12 for the WT-apo, n = 9 for G93A vaccinations. **(D)** Ab titers against G93A SOD1 protein. Sera from vaccinated mice (day 120 and end point) were analyzed by ELISA. The WT-apo SOD1 vaccine induced Ab against G93A SOD1 as well as the G93A-apo SOD1 did even at the end point. *$p < 0.01$ versus saline-injected mice at day 120; $^{\#}p < 0.01$ versus saline-injected mice at end point by 1-way analysis of variance with Bonferroni post hoc test. **(E, F)** Correlation analysis between Ab titer and clinical score including rotarod performance **(E)** and life span **(F)**. Antibodies in both the G93A-apo and the WT-apo vaccination were positively correlated with the onset timing of paralysis **(E)**. The WT-apo SOD1 vaccination was positively correlated with longevity ($p = 0.00441$, Spearman $r = 0.6768$); the G93A-apo SOD1 vaccine displayed a lower value for Spearman r (0.0887).

TABLE. Effect of Vaccinations on Days of Disease Onset and Survival of G93A Mice

Vaccine	Saline	WT-Apo	G93A-Apo		Saline	WT-Apo	G93A-Apo
Median survival	274	288	287.5	Mean survival (d)	272 ± 3.9	291 ± 7.9	283 ± 4.9
Median onset of rotarod impairment	225	243.5	249	Mean onset of Rotarod impairment	228 ± 5.4	239 ± 7.5	249 ± 6.2
Median onset BW loss	212	234	228	Mean onset BW loss	212 ± 6.2	247 ± 10.6	233 ± 5.9
Effect on survival	—	14	13.5	Effect on survival	—	19	11
Effect on rotarod impairment onset	—	18.5	24	Effect on rotarod impairment onset	—	11	21
Effect on onset BW loss	—	22	16	Effect for onset BW	—	35	21

The effect of vaccination with recombinant G93A-apo or the WT-apo SOD1 protein on the delay of the disease onset or extension of the life span of low-copy G93A SOD1 (G93AGur^{dl}) mice. The left columns are median survival or median onset determined by Kaplan-Myer curves. Data in the right columns show the mean days from each vaccination ± SEM (n = 13 for saline, n = 12 for WT, and n = 9 for G93A).

Effect on survival or onset of impaired rotarod performance and body weight (BW) loss were obtained by subtracting the date for saline injection from those for the WT-apo or the G93A-apo SOD1 vaccination. Time of disease onset was determined by BW loss and rotarod performance. All data are days.

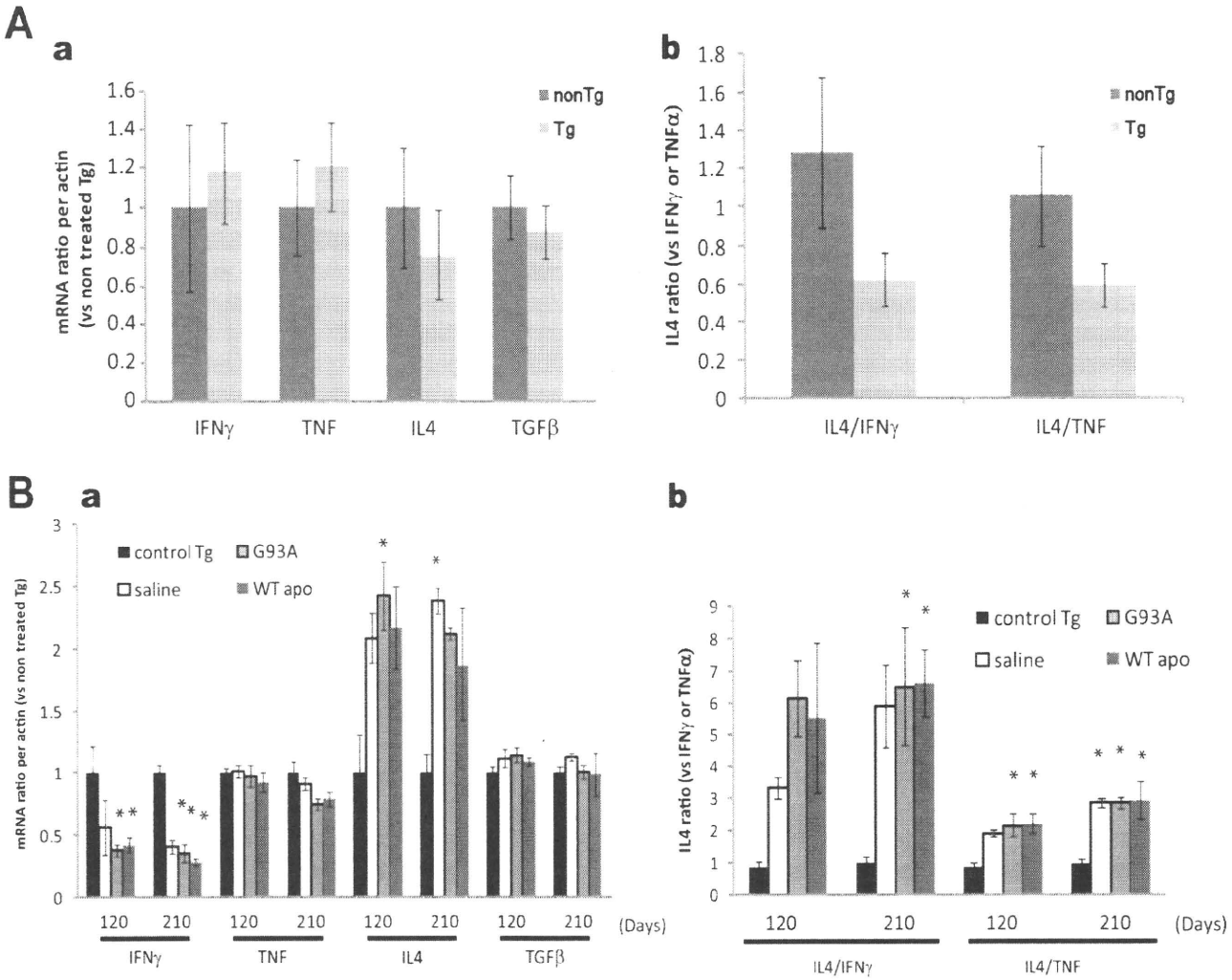

FIGURE 3. Induction of T_H2 deviation in the spinal cord by superoxide dismutase 1 (SOD1) vaccination. **(A, a)** Real-time polymerase chain reaction analysis of mRNA of interferon-γ (IFNγ), tumor necrosis factor (TNF), interleukin-4 (IL-4), and transforming growth factor β (TGFb) in spinal cord tissues from nontransgenic (Tg) wild-type (WT) and nontreated Tg mice at the early presymptomatic stage (day 120). The mean mRNA of each cytokine standardized by actin mRNA is shown. **(A, b)** The ratio of IL-4 to IFNγ or to TNF in each mouse was averaged in each group to estimate the T_H2/T_H1 milieu. The mean IL-4/IFNγ or IL-4/TNF ratio shows a decrease in presymptomatic Tg mice (mean ± SEM, n = 3 for non-Tg mice, and n = 4 for Tg mice). **(B, a)** Real-time polymerase chain reaction analysis of the same cytokines in the spinal cord of the vaccinated mice with WT or G93A SOD1 proteins or saline plus Ribi adjuvant and nontreated Tg controls. **(B, b)** The ratio of IL-4/IFNγ or IL-4/TNF showing that the SOD1 efficiently induced T_H2 protective immunity by inhibiting IFNγ and provoking IL-4. *$p < 0.05$ versus nontreated Tg controls by 1-way analysis of variance with Bonferroni post hoc test (mean ± SEM, n = 3–4 mice).

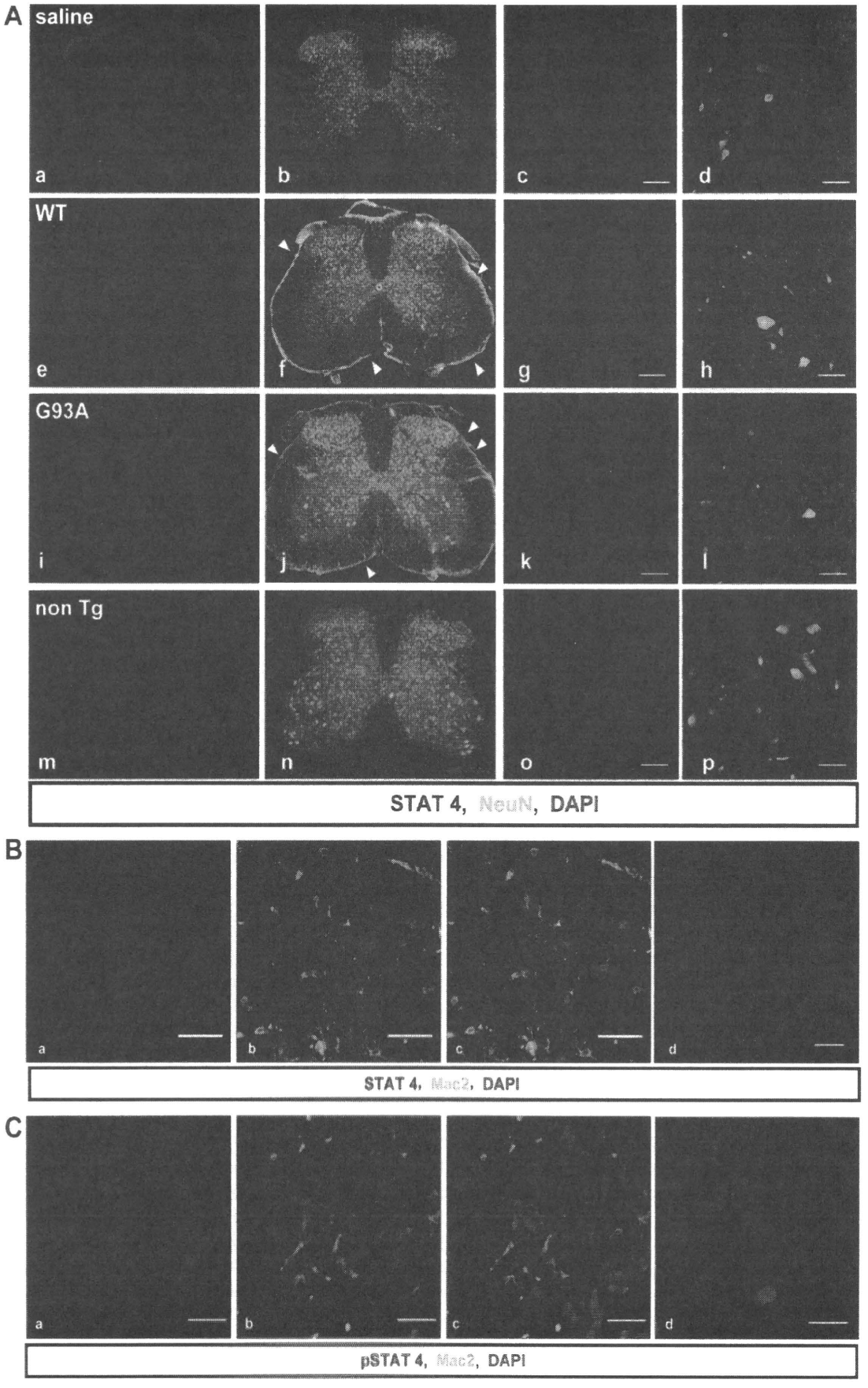

Enzyme-Linked Immunosorbent Assay

At the ages of 120 days, 210 days, or at the end point, sera were obtained for antibody titration for total IgG, IgG1, IgG2b, and IgG2c against G93A SOD1 protein by enzyme-linked immunosorbent assay (ELISA) as previously described (10), with minor modifications (Methods, Supplemental Digital Content 1, http://links.lww.com/NEN/A178).

Immunofluorescent Analysis

The spinal cords at the level of L4-L5 were resected from 275-day-old mice after perfusion with 4% paraformaldehyde. The sections were incubated in the same fixative for 4 hours and subsequently in PBS containing 20% sucrose and 0.1% sodium azide at 4°C. Cryosections 24 μm thick were incubated with a mixture of primary antibodies and subsequently with a mixture of corresponding secondary antibodies labeled with Alexa 488 or 594 (Invitrogen, Carlsbad, CA). For counterstaining, 4,6-diamidino-2-phenylindole dihydrochloride (Nacalai Tesque) was used. The number of remaining motor neurons in the spinal cord was obtained from averaged count of large NeuN+ cells (<20 μm of the soma) in the anterior horn from 3 samples per mouse. Fluorescent images were obtained using a fluorescent microscope (Keyence, Mississauga, Canada) or a confocal laser microscope equipped with the software EZ-C1 (Nikon, Tokyo, Japan). Antibody information is provided in Methods, Supplemental Digital Content 1, http://links.lww.com/NEN/A178.

Serum Cytokine Quantification

Serum concentrations of TNF, IFNγ, and IL-4 were determined using suspension array system (Bio-Plex Pro Mouse Cytokine; BioRad, Hercules, CA) according to the manufacturer's protocol (Methods, Supplemental Digital Content 1, http://links.lww.com/NEN/A178).

Cytokine Profiling in the Spleen and the Spinal Cord by Real-Time Polymerase Chain Reaction

Cytokines and transcription factors including IFNγ, TNF, transforming growth factor β1 (TGFβ), IL-4, forkhead box P3, and RAR-related orphan receptor γ were investigated for their messenger RNA (mRNA) expression level by real-time polymerase chain reaction (PCR) system, as described with minor modifications (26). On days 120 and 210, total RNA was purified using TRIzol and RNA purification kit (Invitrogen), and an equal amount of total RNA was reacted with reverse transcriptase (Superscript III; Invitrogen) to generate complementary DNA (cDNA). mRNA of cytokines or marker molecules for $CD4^+$ T lymphocytes was analyzed by real-time PCR using the SYBR green system (Roche, Basel, Switzerland). The cDNA level of the target molecules was normalized to that of actin. Detailed procedures including primer sequences are in Methods, Supplemental Digital Content 1, http://links.lww.com/NEN/A178.

Statistics

The survival and clinical onset data were analyzed by Kaplan-Meyer curve and log-rank tests. The effect of a single factor on the difference among 3 or more groups was determined by 1-way analysis of variance (ANOVA) with Bonferroni post hoc test. Comparisons between 2 groups were analyzed by unpaired *t* test. $p < 0.05$ was judged to be significant.

RESULTS

Characterization of Recombinant SOD1s

The purities of recombinant SOD1s were more than 95%, as determined by SDS-PAGE (data not shown). To investigate the precise molecular weight of SOD1 proteins of as-isolated and nonmetallated state (i.e. WT-apo or G93A-apo) versus the holo-state, we performed molecular-size filtration chromatography because it is thought that apo-SOD1s are constantly monomers (27). However, both apo- and holo-SOD1s are dimeric, although the WT-apo sample appeared to contain some monomer form (Fig. 1). Moreover, the elution times of WT-apo and G93-apoA were slightly faster than those of the holo-types, which could reflect looser structures of apo-SOD1s.

Vaccination With Recombinant WT-Apo SOD1 Extends the Life Expectancy and Delays Disease Onset

$G93AGur^{dl}$ mice were immunized with recombinant G93A-apo SOD1 or WT-apo SOD1 using Ribi adjuvant. Recombinant WT-apo SOD1 was used because of its broader applications regardless of mutation types in SOD1 gene and because, like mutant SOD1, it is misfolded (22). The G93A-apo vaccine significantly delayed the onset of paralysis assessed by BW change and rotarod performance tests (Figs. 2A, B). The WT-apo SOD1 vaccination also significantly suppressed BW loss and showed a trend to preserving the rotarod performance, although this was not significant. The difference of onset time was 18 or 22 days in the WT-apo- and 24 or 16 days in the G93A-apo vaccinated mice, as assessed rotarod tests or BW change, respectively (Table). In addition, both vaccines prolonged the life spans compared with saline/adjuvant–injected controls by 14 and 13.5 days for WT-apo and G93A-apo vaccine, respectively. The log-rank test determined statistical significance only for the WT-apo SOD1 vaccinations ($p = 0.0183$ for the WT-apo; $p = 0.0720$ for the G93A-apo). Notably, the mean life span

FIGURE 4. Signal transducers and activators of transcription 4 (STAT4), a transcription factor for interferon-γ (IFNγ), is abundantly expressed in active microglia of G93A transgenic (Tg) mice. **(A)** Double immunostaining for STAT4 (red) and NeuN (green) in the spinal cord of vaccinated 275-day-old mice. The left 2 columns **(a, b, e, f, i, j, m, n)** and the right 2 columns **(c, d, g, h, k, l, o, p)** are images obtained from the fluorescent microscope and confocal laser microscope, respectively. Expression of STAT4 does not merge with NeuN. Scale bar = 50 μm. **(B, C)** Confocal micrographs of double immunofluorescent analysis for STAT and Mac2 or phosphorylated STAT4 and Mac2 in the spinal cord of $G93AGur^{dl}$ mice. **(a–c)** Saline/adjuvant-injected $G93AGur^{dl}$ mice (30 weeks). **(d)** Non-Tg littermate. Scale bar = 30 μm.

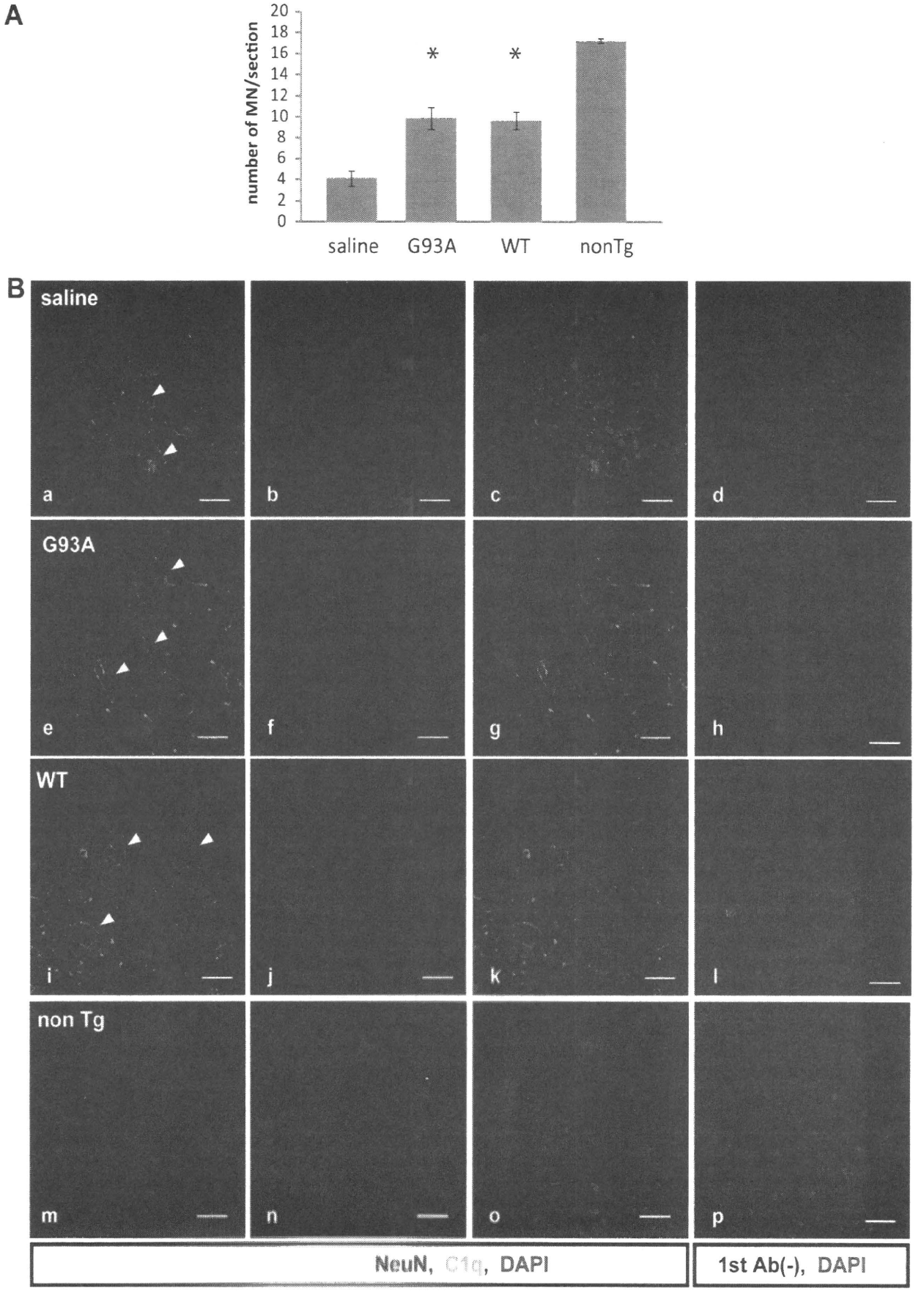

indicated that there were shorter durations of suffering in G93A-apo–vaccinated mice (Fig. 2C; Table).

We next investigated whether the antibody titer correlated with the therapeutic benefit. The WT-apo and the G93A vaccination induced high titers of anti-G93A SOD1 antibody compared with the native SOD1 vaccination or the saline control (Fig. 2D). The WT-apo vaccine showed a significant positive correlation between the life span and antibody titer ($r = 0.5758$, $p = 0.0041$ by Spearman r) and a trend toward a positive correlation of rotarod testing (Fig. 2E; $r = 0.539$, $p = 0.0569$ by Spearman r). The G93A-apo vaccine showed no significant correlation with either the onset timing (rotarod and BW loss) or survival (Figs. 2E, F). The disease duration was not associated with antibody titer in either the WT-apo or G93A-apo vaccine groups (not shown).

SOD1 Vaccination Potentiates Protective Immunity in the Spinal Cord

mRNA levels of IFNγ, TNF, and IL-4 were determined in the spinal cords of presymptomatic nontreated G93A SOD1 Tg mice (120 days old; n = 3) and non-Tg WT littermates (n = 5). There were slightly higher levels of IFNγ and TNF and lower levels of IL-4 in G93A Tg mice versus non-Tg age-matched mice (Fig. 3Aa). The ratios of IL-4 to IFNγ (IL-4/IFNγ) or TNF (IL-4/TNF), (termed "T_H2/T_H1 ratios") were much lower in the Tg mice (Fig. 3Ab). Comparison between SOD1- or saline plus adjuvant–vaccinated groups and nontreated Tg mice showed a significant reduction of IFNγ in both SOD1 vaccinations versus nontreated G93A Tg controls. Interleukin-4 mRNA was markedly elevated by the SOD1 vaccinations on both days 120 and 210, but only the G93A vaccination on day 120 was statistically significant (by 1-way ANOVA, Bonferroni post hoc test). The saline/adjuvant injection provided an effect comparable to that of the SOD1 vaccination in reducing IFNγ and upregulating IL-4 (Fig. 3Ba). The T_H1/T_H2 milieu is critically influenced by the adjuvant as well as by antigens, and the MPL/TDM adjuvant used has been reported to favor a T_H2 rather than T_H1 milieu (28).

Signal Transducers and Activators of Transcription 4 Induction in Active Microglia in the Spinal Cord

The role of IFNγ in ALS pathogenesis is controversial (14, 29–31). Therefore, we examined the expression pattern of IFNγ in spinal cords of mutant SOD1 Tg mice. Immunohistochemical analysis was performed with an antibody against signal transducers and activators of transcription 4 (STAT4), an activator for transcription of IFNγ under the stimulation of IL-12. There was STAT4 immunoreactivity in the spinal cord of mutant SOD1 Tg mice with or without vaccination (Fig. 4A). Notably, the lamina I in the dorsal horn, which receives nociceptive input, was markedly STAT4+ in both Tg and non-Tg mice (Fig. 4A, a, b, e, f, i, j, m, n). These cells were also NeuN+ (not shown), which might imply a role for IFNγ in pain generation to nociceptive stimulation (32). However, the STAT4+ cells in other areas, including the anterior horn are not costained with anti-NeuN antibody (Fig. 4A, c, d, g, h, k, l, o, p). Therefore, we performed double immunofluorescent staining using antibodies against STAT4 and Mac2. STAT4 was exclusively expressed in Mac2+ active microglia (Fig. 4B). Because phosphorylation is required to activate STAT4 for IFNγ transcription, we examined the presence of phosphorylated STAT4 (pSTAT4) by double immunofluorescent study and found that certain populations of active microglia were pSTAT4+ (Fig. 4C). There was no difference in STAT4 or pSTAT4 levels between vaccinated or nonvaccinated mice (not shown), but the presence of STAT4 in microglia provides evidence that spinal motor neurons are affected by IFNγ from activated microglia. Notably, the fluorescent antimouse IgG antibodies showed meningeal enhancement only in SOD1 vaccinated mice (Fig. 4A, arrowheads), suggesting that vaccine-generated antibodies can reach the spinal cord.

Vaccination With G93A-Apo or WT-Apo SOD1 Attenuates Motor Neuron Loss and Induces Complement C1q Deposition

We next investigated whether the beneficial effect of the vaccination with the G93A-apo or the WT-apo SOD1 correlated with motor neuron protection by counting of NeuN+ remaining anterior horn cells in 275-day-old Tg mice. Both vaccinations with the G93A-apo and the WT-apo significantly attenuated motor neuron loss (Fig. 5A), whereas there was no significant difference in the number of active microglia cells stained by anti–Mac-2 between saline and SOD1 vaccinations was observed (Figure, Supplemental Digital Content 2, http://links.lww.com/NEN/A179).

We then studied the activation of the classic pathway of complement system after vaccination in mice of the same age. C1q, which binds to antigen-antibody complexes at the immunoglobulin Fc domain, is upregulated around motor neurons in SOD1 mutant models before disease onset, suggesting that "danger molecules" are leaked from degenerating motor neurons (33). Double immunofluorescent staining with rat monoclonal anti-C1q and mouse monoclonal anti-NeuN detected C1q around motor neurons in both SOD1-vaccinated and saline-control $G93AGur^{dl}$ mice, but not in age-matched non-Tg littermates. More prominent C1q deposition was detected in SOD1 vaccinated mice than in saline/adjuvant controls (Fig. 5B). These data indicate that the apo-SOD1 vaccination activates the classic pathway in the spinal cord. Because chromogranin interacts with mutant SOD1, promotes

FIGURE 5. Superoxide dismutase 1 (SOD1) vaccination attenuates motor neuron (MN) loss and induces complement deposition around MNs. **(A)** MN count in the spinal cord of vaccinated 275-day-old mice. NeuN+ large anterior horn neurons (>20 μm in size) were counted in 3 slices per mouse; mean numbers per slice are shown. *$p < 0.05$ by 1-way analysis of variance of Bonferroni test (n = 9 for transgenic [Tg], n = 4 for non-Tg; WT = wild-type. **(B)** Induction of complement C1q deposition around MNs by SOD1 vaccination. Confocal micrographs of the spinal cord slices of the vaccinated mice (30 weeks) stained with antibodies against NeuN (red, mouse monoclonal) and C1q (green, rat monoclonal). C1q staining surrounding MNs are indicated with arrowheads; **d, h, l, p** show negative controls in which primary antibodies were eliminated. Scale bar = 30 μm.

its secretion, and activates microglia (9), the complex formation comprising mutant SOD1–anti-SOD1 antibody-C1q may be facilitated by the SOD1 vaccination.

WT-Apo SOD1 Vaccination Induces a Higher T_H2/T_H1 Milieu Than G93A Vaccination

There were differences in the slowing of the progression in Tg mice between the WT-apo and the G93A SOD1 vaccinations. Because the antibody titer in the G93A-apo vaccination unexpectedly showed no correlation with disease onset or life span as opposed to the WT-apo (Figs. 2E, F), we compared the IgG subclasses induced by the WT-apo and G93A-apo vaccines. Sera of SOD1-vaccinated mice were analyzed on days 120 and 210 by ELISA for IgG1, 2b, and 2c titers. Both the WT-apo and the G93A-apo vaccines induced considerable amounts of each subclass and the G93A vaccination induced more IgG than the WT vaccination. Overall, the difference between the 2 vaccines was statistically significant only on day 120 for IgG1 and day 210 for IgG2b and IgG2c (Fig. 6A, $p < 0.05$ by unpaired t test). The mean ratios of IgG1 to IgG2c (IgG1/IgG2c) (an indicator of the T_H2/T_H1 milieu) were not significantly different between WT and G93A vaccinations on day 120, but on day 210, this ratio was significantly higher in the WT-apo vaccination than in the G93A (Fig. 6Ab, $p < 0.05$ by 1-way ANOVA).

We further measured the quantity of serum cytokines induced by these SOD1 vaccinations using a suspension array system. The antisera from immunized mice with WT or G93A SOD1 vaccine (n = 3/group) on day 120 was analyzed for TNF, IFNγ, and IL-4. The G93A-apo vaccination induced more of the T_H1 cytokines TNF and IFNγ compared with the WT-apo vaccination (Fig. 6B). Interleukin-4 levels were below the detection limit (0.59 pg/mL) in either non-Tg or Tg mice regardless of the type of the vaccination. The analysis of the spleen tissues of the same mice for mRNA quantity of TNF, IFNγ, IL-4, and TGFβ by real-time PCR revealed a clear trend in which IL-4 mRNA in the WT or the G93A vaccination was higher than that in the saline control on day 120. The G93A vaccination tended to induce higher IL-4 than the WT did on day 120. On day 210, IL-4 mRNA remained high in the WT but not in the G93A vaccination sera (Figure, part A, Supplemental Digital Content 2, http://links.lww.com/NEN/A179). No significant differences in expression levels of forkhead box P3 or RAR-related orphan receptor γt, a marker for regulatory T-cell or a T_H1 7 cells, respectively, between control and vaccinated groups were observed (data not shown).

We then analyzed the relationship between IgG subclass and the therapeutic effect of the vaccinations. In the WT-apo vaccination there was a positive correlation between IgG2b titer and the date of the onset (Figure, part B, Supplemental Digital Content 3, http://links.lww.com/NEN/A180, b;

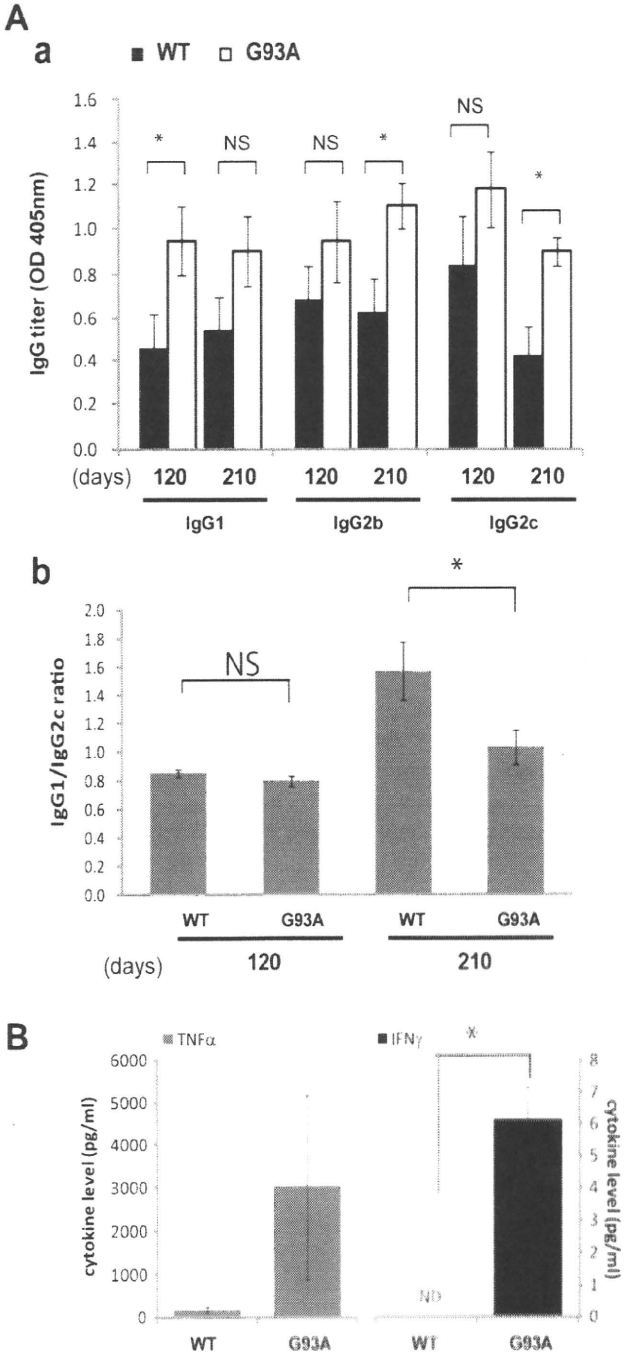

FIGURE 6. Analysis of sera for acquired immunity by superoxide dismutase 1 (SOD1) vaccination. **(A, a)** ELISA for IgG subclasses induced by the SOD1 vaccination. The titer for IgG1, 2b, and 2c against the G93A-apo SOD1 was obtained from sera of wild-type (WT) and G93A SOD1-vaccinated mice at day 120 and 210 and expressed as optical density (OD) 405 nm (mean ± SEM; each group, n = 4 or 5). *$p < 0.05$, NS indicates not significant by unpaired t test. **(A, b)** The ratio of IgG1 to IgG2c (IgG1/IgG2c) was obtained in each mouse and the data averaged (mean ± SEM for each group, n = 4 or 5). *$p < 0.05$ by 1-way analysis of variance with Bonferroni post hoc test. **(B)** Serum cytokine concentrations. Sera from WT or G93A SOD1 vaccination (n = 3) were analyzed for the quantification of interferon gamma (IFNγ) and tumor necrosis factor (TNF) using a suspension array system. Each bar shows the mean concentration from 3 mice ± SEM. *$p < 0.05$ by unpaired t test. ND indicates not detected (under the lowest value of standard curve (0.17 pg/mL).